RSC Advances

PAPER

View Article Online
View Journal | View Issue

Cite this: *RSC Adv.*, 2026, **16**, 27090

Novel nanomagnetite doped sugarcane bagasse biochar biocomposite for efficient removal of toxic heavy metal ions from wastewater

Magda A. Akl, * Aya G. Mostafa and Asmaa A. Serage

Efficient enrichment and remediation of heavy metals from real wastewater and contaminated soil, both of which frequently contain high concentrations of competing ions, remain significant challenges. Producing advanced carbon-based materials that efficiently remove contaminants from water is crucial for environmental remediation and public health. This investigation describes the concurrent activation and magnetization processes used to synthesize Mag@SAC, a magnetic sugarcane activated carbon, from carbonized sugarcane bagasse (SB) using Fe^{3+} and Fe^{2+} ions. The Mag@SAC biocomposite was thoroughly characterized using Brunauer–Emmett–Teller (BET) and N_2 adsorption isotherm analysis, point of zero charge (pH_{PZC}), elemental analysis, Scanning electron microscopy (SEM), Fourier transform infrared spectroscopy (FTIR), and Thermogravimetric analysis (TGA). The as-prepared Mag@SAC was applied to remove toxic heavy metals, Pb^{2+} and Hg^{2+} from solutions, with easy separation achieved by simply applying an external magnet. The adsorption of Pb^{2+} and Hg^{2+} onto Mag@SAC biocomposite follows pseudo-second-order (PSO) kinetics and is best described by the Langmuir isotherm, indicating spontaneous, monolayer chemisorption. This process is supported by a high correlation coefficient ($R^2 \geq 0.999$) and low error functions. Maximum adsorption capacities of 90.82 mg g^{-1} for Pb^{2+} and 164.20 mg g^{-1} for Hg^{2+} were obtained under optimal conditions. Thermodynamic analysis indicates that the adsorption of Hg^{2+} onto Mag@SAC is spontaneous and endothermic, whereas the adsorption of Pb^{2+} is spontaneous and exothermic. The Mag@SAC biocomposite can be successfully regenerated up to the 5th cycle. The mechanisms of adsorption of Pb^{2+} and Hg^{2+} onto the Mag@SAC were elucidated.

Received 17th April 2026
Accepted 11th May 2026

DOI: 10.1039/d6ra03304k

rsc.li/rsc-advances

1 Introduction

The depletion of water resources constitutes a major global challenge. In recent years, global warming and climate change have intensified the reduction of essential water supplies, prompting governments to prioritize water treatment initiatives. Such initiatives frequently include directives for water treatment and desalination facilities to utilize various bioadsorbents.[1]

Chemical water contamination may originate from waste generated by chemical manufacturing, electroplating, dye and textile production, tanneries, oil extraction, mining, and smelting. When heavy metals seep into rivers and lakes, they threaten not only the health of people worldwide but also the delicate balance of aquatic life. Heavy metals, including lead, mercury, cadmium, and chromium, notorious for their extreme toxicity, can silently accumulate in the body and trigger a host of health issues. These metals may cause gradual physical, neurological, and muscular problems that mimic conditions such as Alzheimer's, Parkinson's, Scoliosis, and multiple sclerosis. Because heavy metals do not break down into harmless substances, their lingering presence can even increase the risk of cancer.[2–4]

Lead and mercury are among the most widely studied heavy metals worldwide due to their high toxicity and tendency to accumulate in water and food resources. Human beings can be exposed to them from various sources, including the plastic industry, oil refineries, pulp mills, the glass end caps of spent fluorescent lamps, phosphor powder, the cement industry, and other industries.[5,6] Various strategies were applied to eliminate them from wastewater, including bioremediation,[7] coagulation,[8] chemical precipitation,[9] membrane filtration,[10] solvent extraction,[11] electrolysis,[12] reverse osmosis,[13] ion exchange,[14] and adsorption.[15]

The adsorption technique is considered a promising strategy for water treatment from heavy metal contamination because of its low cost, low energy consumption, simplicity, and capacity to manage large-scale systems.[16,17] In this study, we use the adsorption process with eco-friendly nanomagnetite-modified biochar prepared from sugarcane bagasse bioresidues. SB has been selected as a cost-effective bio-residue for the preparation of activated carbon due to its demonstrated potential as a biosorbent for the removal of metal ions from wastewater.[18,19] Its

Department of Chemistry, Faculty of Science, Mansoura University, Mansoura 35516, Egypt. E-mail: magdaakl@yahoo.com

abundance of hydroxyl groups creates active sites that encourage ion exchange and complexation with metal ions, boosting its hydrophilicity and enhancing its ability to interact with metal ions in water.[20,21]

This research harnesses the untapped potential of SB, an abundant and affordable agro-residue, by grafting it with Fe_3O_4 magnetic nanoparticles. The result is a powerful Mag@SAC that excels at adsorbing heavy metal ions, such as Pb^{2+} and Hg^{2+}.[22] Pollutants in various water sources can chemically interact with SB, which contains cellulose, hemicellulose, and lignin, alongside hydroxyl-containing macromolecules.[23,24] Akl and Serag reported the effective immobilization of chitosan onto biochar derived from SB, resulting in the SCNC biosorbent, which was used to remove Congo red from wastewater.[25] SB was modified with sulfonic groups to create a biosorbent for the adsorption of cationic dyes.[26] Magnetic activated carbon particles are an emerging adsorbent valued for their high surface area and favorable magnetic properties.[27]

We present a simple, cost-effective method to modify SB biochar for reuse in the removal of metal ions from water. Results show that adding Fe_3O_4 magnetic nanoparticles increases sugarcane bagasse biochar's adsorption capacity for Pb^{2+} and Hg^{2+}. The magnetic particles (Fe_3O_4) also facilitate the separation of the adsorbent from the metal solution, which benefits practical use.

The novelty of this work lies not only in the use of magnetite-based biochar for metal removal but also in the integrated preparation strategy. Controlled pyrolysis converts native SB into SCB biochar, followed by high-temperature steam activation to develop a well-defined porous structure in Mag@SAC. Steam activation is more eco-friendly than conventional chemical methods and promotes the formation of a hierarchical pore system. Fe_3O_4 nanoparticles are incorporated through *in situ* co-precipitation, ensuring uniform dispersion and strong interaction with the biochar surface. This combined approach produces a magnetically separable adsorbent with improved textural properties and active sites for heavy-metal adsorption.

Addressing the identified research gaps, this study presents the rational design of a magnetically supported sugarcane bagasse biochar biocomposite. This material integrates adsorptive biochar with magnetic Fe_3O_4 nanoparticles to enhance the purification of water contaminated with heavy metals. Accordingly, the following objectives were established to evaluate the implementation and significance of this investigation: (i) synthesis of a novel magnetic Mag@SAC as a highly efficient nanobiosorbent for the removal of Pb^{2+} and Hg^{2+}; (ii) characterize the Mag@SAC's physico-chemical properties, using various analytical instruments; (iii) systematically investigate the influences of solution pH, Mag@SAC dosage, agitation time, initial concentration, temperature, and coexisting ions on Pb^{2+} and Hg^{2+} removal; (iv) to fit the Pb^{2+} and Hg^{2+} adsorption experimental data to various kinetic and isothermal adsorption models alongside statistical error functions; (v) to comparatively evaluate the removal efficiency, feasibility, and reusability of the Mag@SAC relative to other adsorbents; and (vi) to estimate the Pb^{2+} and Hg^{2+} adsorption mechanism onto the Mag@SAC biocomposite surface.

2 Materials and methods

2.1. Materials

All employed chemicals in the present investigation were of analytical grade (AR), obtained from Sigma-Aldrich company and utilized without further purification. To prepare a 1000 mg L^{-1} stock solution of Pb^{2+} and Hg^{2+}, 1.598 g and 1.344 g of $Pb(NO_3)_2$ and $HgCl_2$, respectively, were dissolved in deionized water. Then, a few drops of concentrated HNO_3 were added to acidify the solution and prevent the metal from hydrolyzing. The investigated magnetite was prepared using $FeCl_3 \cdot 6H_2O$ (AR) and $FeCl_2 \cdot 4H_2O$ (AR), along with sodium hydroxide (NaOH).

2.2. Instrumentation and characterization

Nitrogen adsorption–desorption is employed to characterize the porous structure, and the Brunauer–Emmett–Teller (BET) theory is applied to estimate the Mag@SAC's surface area (S_{BET}, $m^2\ g^{-1}$). These measurements are based on gas adsorption measurements using the QUANTACHROME NOVA 2000 Series analyzer, which employs nitrogen chilled to its boiling point (77 K).[28] The point of zero charge (pH_{PZC}) of the Mag@SAC was determined using the pH reported method.[29] A weight (0.1–0.15 g) of the Mag@SAC was shaken for 48 hours with 0.01 M NaCl solutions, whose pH was adjusted between 2 and 12 using 0.05 M HCl or 0.05 M NaOH. The final pH was measured and plotted against the change in pH (ΔpH). The surface morphology of the Mag@SAC sample was characterized using a JSE-T20 (JEOL, Japan) microscope. Fourier transform infrared (FT-IR) spectral analysis was conducted with a Shimadzu 5800 FT-IR spectrometer across a wavelength range of 4000 to 400 cm^{-1}. Thermo gravimetric analysis (TGA) was performed as the changes in the mass of nano-magnetite modified biochar as a function of temperature were measured by TGA/DTG curve using a Shimadzu (Japan) model under N_2 gas flow with a heating rate of 10 °C min^{-1}. The saturation magnetization (MS) of Mag@SAC at room temperature was measured using the advanced Cryogenic Limited Physical Property Measurement System (PPMS) for precise results. A Neodymium N52 magnet (50 × 20 × 7 mm, 15 kg pulling force) was utilized to separate Mag@SAC loaded with metal ions after sorption. The concentrations of residual Pb^{2+} and Hg^{2+} in solution are measured spectrophotometrically using a UV-Vis spectrophotometer (JENWAY Co., Ltd, UK) at λ_{max} values of 520 nm and 522 nm, respectively, with PAR reagent. Before conducting the analysis, calibration curves for Pb^{2+} and Hg^{2+} with PAR were established using standard solutions, demonstrating strong linearity (R^2 > 0.99; Fig. S1).

2.3. Preparations

2.3.1. Steam-activated carbon (SAC). Initially, the SB precursor was dried in the sunlight and subsequently cut into small pieces. The material was then washed multiple times with

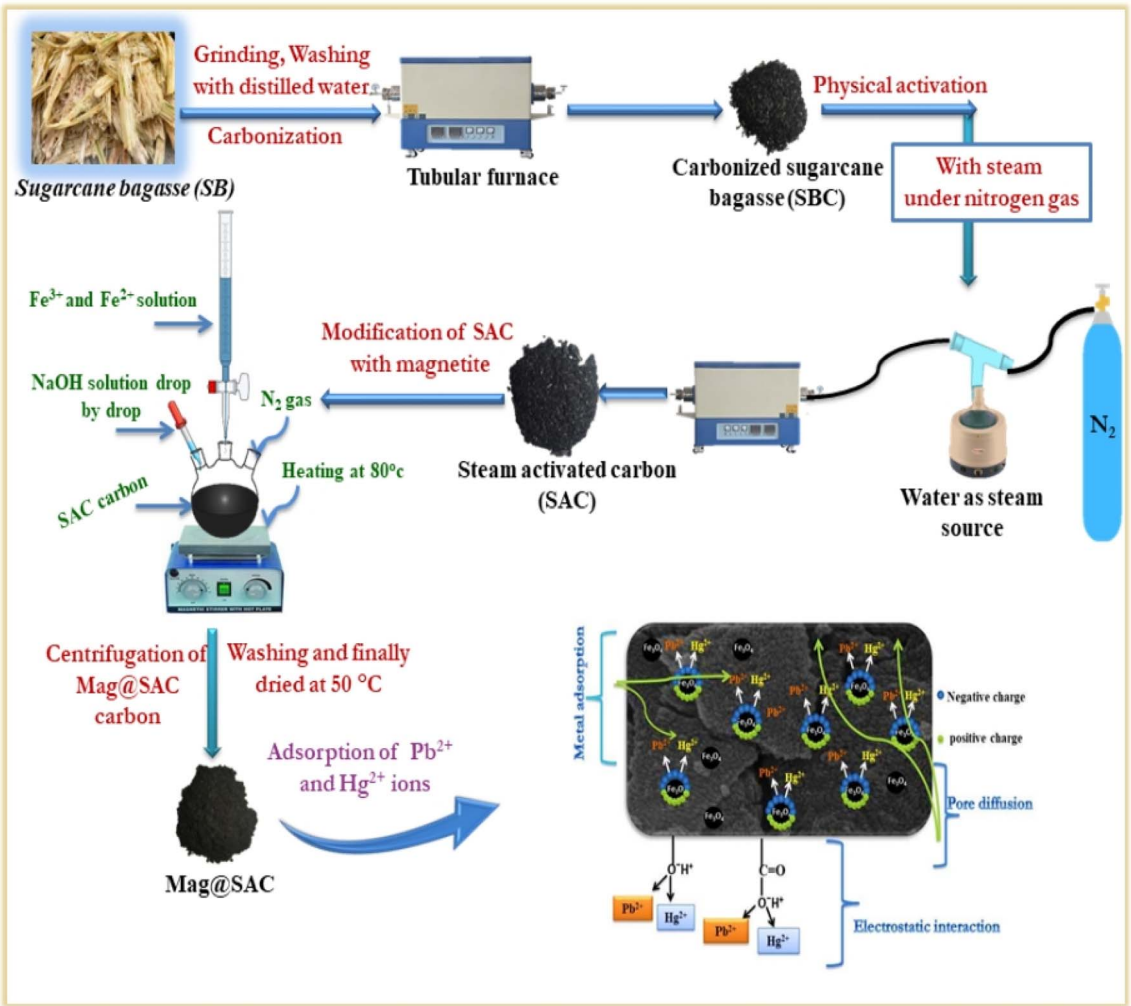

Fig. 1 Preparation of Mag@SAC biocomposite.

a 1–5% HCl solution to remove dirt and extraneous matter. Afterward, the material was rinsed with deionized water until the supernatant turned neutral. It was then crushed, ground, and sieved to yield fine particles with a particle size less than 0.45 mm. The precursors were oven-dried at 105–110 °C overnight or until fully dry.

The dried precursors (SB) were calcined in a stainless-steel reactor under an oxygen-free atmosphere at about 600 °C for 2 hours. The sample temperature was monitored with a K-type thermocouple and regulated with a digital temperature controller. The sugarcane bagasse biochar (SBC) was then physically activated by steam gasification to produce physically activated carbon (SAC) at 900 °C by adjusting the time of activation for about 26 min using a horizontal tubular furnace with a length of 450 mm and an internal diameter of 65 mm was used for gasifying (SBC). The steam-activating agent is generated by injecting water into a heated reactor, where it evaporates to produce water vapor. Nitrogen gas at a flow rate of 100 $cm^3\ min^{-1}$, measured at room temperature, serves as the carrier gas. The water vapor flow is maintained at a constant rate for 36 min.[28] The final yield was calculated at 26%.

2.3.2. Preparation of nano-magnetite grafted sugarcane bagasse biochar (Mag@SAC) biocomposite. The SAC undergoes an *in situ* reaction to prepare activated carbon modified with Fe_3O_4. About 2 g of SAC sample was stirred with (1.5 M) of NaOH, then the iron salt solution containing $FeCl_2 \cdot 4H_2O$ and $FeCl_3 \cdot 6H_2O$ with a 1 : 2 (Fe^{2+} : Fe^{3+}) molar ratio dissolved in concentrated HCl (12 M) was added dropwise on activated carbon to precipitate Fe_3O_4 nanoparticles on the surface of activated carbon at 80 °C under a flow of nitrogen gas.[30] Mag@SAC was washed with demineralized water using a dialysis system and subsequently dried in an oven at 50 °C overnight. Fig. 1 provides a schematic illustration of the Mag@SAC preparation.

2.4. Batch adsorption studies

The removal of Pb^{2+} and Hg^{2+} ions by the Mag@SAC was studied through batch adsorption experiments. For each test, 25 mL of either Pb^{2+} or Hg^{2+} solution was mixed with a measured amount of Mag@SAC in a 50 mL stoppered bottle to initiate adsorption. Experimental parameters were

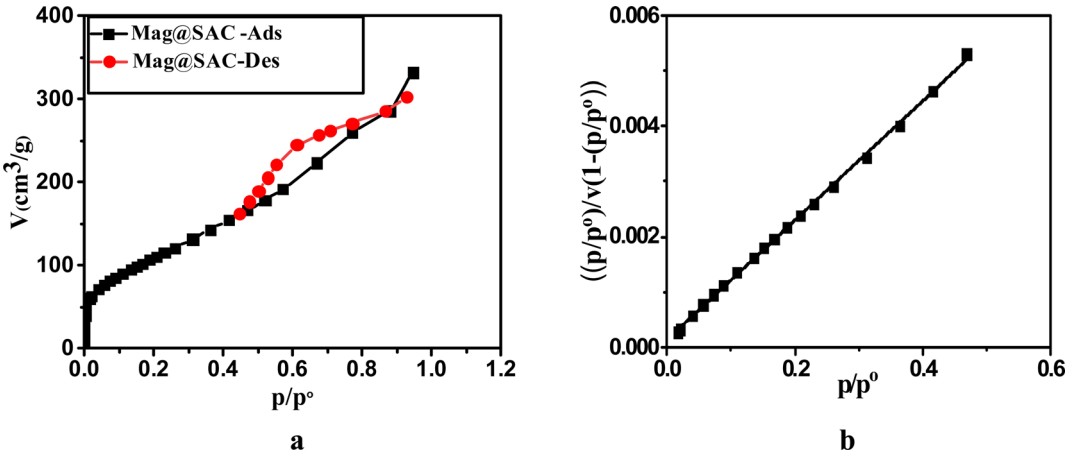

Fig. 2 (a) Nitrogen adsorption–desorption isotherms at 77 K for Mag@SAC and (b) linear plot of BET.

Table 1 The calculated S_{BET} of the prepared Mag@SAC from N_2 adsorption isotherms

Sample	S_{BET} ($m^2\ g^{-1}$)	Total pore volume($cm^3\ g^{-1}$)	Mean pore diameter ($\bar{r}$), Å
Mag@SAC	417.52	0.5132	49.17

systematically varied: pH (1.5–6), metal ion concentrations (5–300 mg L^{-1} for Pb^{2+}, 10–275 mg L^{-1} for Hg^{2+}), Mag@SAC mass (0.005–0.08 g), and oscillation time (5–240 min). The pH was adjusted using diluted HCl or NaOH. Mag@SAC was separated from the solution using an external magnetic field. The PAR reagent measured remaining metal concentrations at 520 nm (Pb^{2+}) and 522 nm (Hg^{2+}). The adsorption capacity of Mag@SAC (q_e, mg g^{-1}) and the removal percentage of Pb^{2+} and Hg^{2+} (R, %) were determined using eqn (1) and (2).[31,32]

$$q_e = \frac{(C_o - C_e)V}{W} \quad (1)$$

$$\%\ R = \frac{(C_o - C_e)}{C_o} \quad (2)$$

C_o and C_e represent the initial and equilibrium Pb^{2+} and Hg^{2+} solution in (mg L^{-1}), respectively. V is the volume of the heavy metal solutions in liters, while W refers to the weight of Mag@SAC in grams. Each experiment was carefully repeated three times to ensure consistent results.

2.4.1. Adsorption isotherms, kinetic, statistical error validity, and thermodynamic investigations

2.4.1.1. Adsorption isotherms. Several adsorption isothermal models have been used to characterize the relationship between equilibrium concentration and adsorption capacity.[33] Adsorption on activated carbons is typically characterized using isotherms, including the linear and nonlinear forms of the Langmuir and the Freundlich models in eqn (3)–(6), respectively.[34]

$$\frac{C_e}{q_e} = \frac{1}{b_1 q_{m1}} + \frac{C_e}{q_{m1}} \quad (3)$$

$$q_e = \frac{q_{m2} b_2 C_e}{1 + b_2 C_e} \quad (4)$$

$$\log q_e = \log K_{F1} + \frac{1}{n}\log C_e \quad (5)$$

$$q_e = K_{F2} C_e^{1/n} \quad (6)$$

C_e (mg L^{-1}) and q_e (mg g^{-1}) represent the equilibrium concentration and adsorbed amount per unit weight of Hg^{2+} and Pb^{2+} on Mag@SAC biocomposite, respectively. The parameter b represents the Langmuir equilibrium constant (L mg^{-1}). K_F ((mg g^{-1})(L $mg^{-1})^{1/n}$) is the Freundlich constant, reflecting the amount of Hg^{2+} and Pb^{2+} adsorbed onto Mag@SAC at unit equilibrium concentration.[26] The n exponent is the Freundlich one, which is essential for evaluating adsorption feasibility.[35]

Table 2 Physicochemical characteristics of the Mag@SAC biocomposite

					Elemental analysis			
Biosorbent	pH of supernatant	pH_{PZC}	Ash%	Moisture%	C (%)	H (%)	N (%)	S (%)
Mag@SAC	7.3	6.9	39.43	6.54	47.501	1.91	—	—

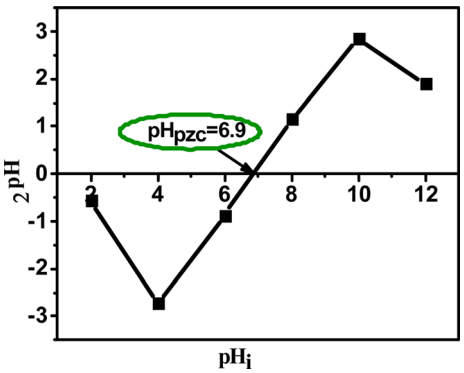

Fig. 3 Point zero charge for Mag@SAC biocomposite.

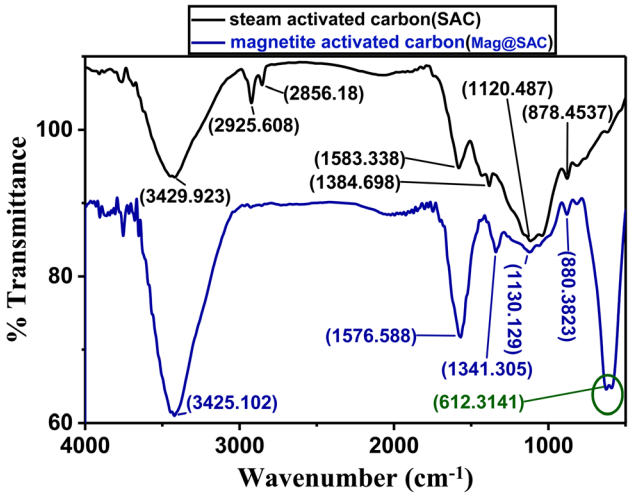

Fig. 5 FTIR spectra of SAC and Mag@SAC.

The $1/n$ parameter is essential for assessing adsorption intensity and surface heterogeneity.[36] Values below 1 indicate a favorable adsorption,[37] whereas higher values suggest increased adsorbate–adsorbent affinity and greater heterogeneity of adsorbent sites.

The R_L, present in eqn (7), is the dimensionless separation parameter that indicates whether adsorption is favorable.

$$R_L = \frac{1}{1 + K_L C_o} \tag{7}$$

C_o represents the highest initial solute concentration, while K_L denotes the Langmuir constant.

2.4.1.2. Adsorption kinetics. Kinetic investigation has been applied to experimental data to determine the adsorption mechanism and its potential rate-controlling step, including mass transfer and chemical reaction. Adsorption kinetic studies for Pb^{2+} and Hg^{2+} on the Mag@SAC sample are investigated using several models. The kinetic data obtained from batch studies have been analyzed using the pseudo-first-order model (PFO), the PSO model, the intraparticle diffusion model (IPD), and the Boyd model, as presented in eqn (8)–(11), respectively.[38–40] The IPD model identifies the diffusion mechanisms and the rate-determining step in adsorption. Kinetic data were analyzed using the expression proposed by Boyd *et al.*[41] to assess whether adsorption occurs through external or intraparticle diffusion.

$$\log(q_{e1} - q_t) = \log q_{e1} - \frac{k_1}{2.303} t \tag{8}$$

$$\frac{t}{q_t} = \frac{1}{k_2 q_{e2}^2} + \frac{1}{q_{e2}} t \tag{9}$$

$$q_t = k_{int} t^{0.5} + c \tag{10}$$

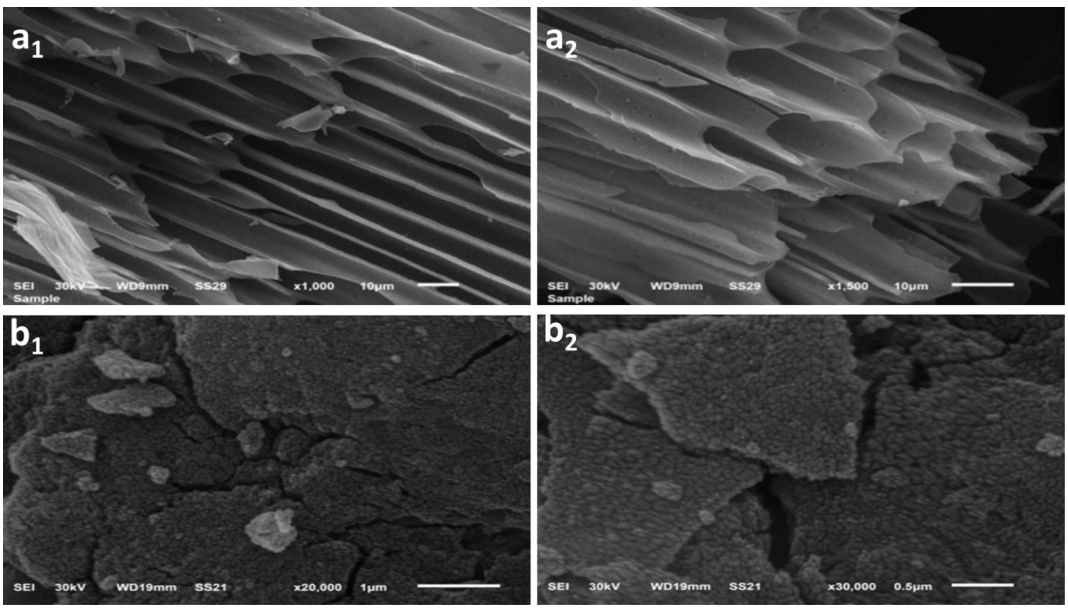

Fig. 4 SEM micrograph of activated carbon, (a_1 & a_2) for SAC, (b_1 & b_2) for Mag@SAC, respectively.

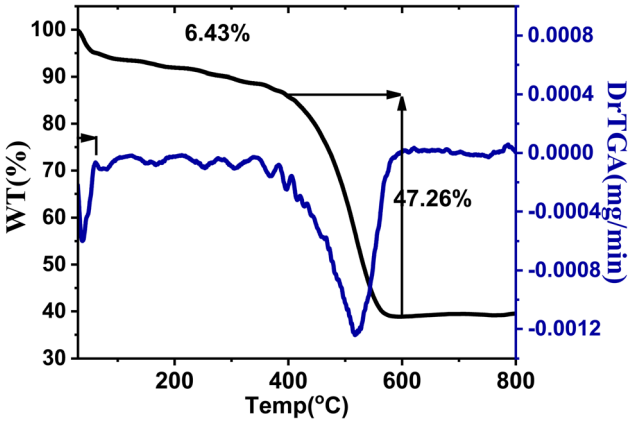

Fig. 6 Thermal analysis of Mag@SAC.

$$F(t) = 1 - \frac{6}{\pi^2}\sum_{n=1}^{\infty}\frac{1}{n^2}\exp\left(-n^2 B(t)\right) \quad (11)$$

q_e (mg g^{-1}) and q_t (mg g^{-1}) represent the amounts of Pb^{2+} and Hg^{2+} adsorbed at equilibrium and at time t (min), respectively. K_2 (g mg^{-1} min^{-1}) and k_{int} are the rate constants for the PSO and IPD models, respectively, while C is an IPD model constant. Where F is the fraction of solute adsorbed at any time (t), it can be evaluated using eqn (12). $B(t)$ is a mathematical function of F, while n is an integer that defines the infinite series solution.

$$F = \frac{q_t}{q_e} \quad (12)$$

The following possibilities were obtained by Reichenberg (eqn (13) and (14)):[42]

For F values < 0.85;

$$B(t) = -0.4977 - \ln(1 - F) \quad (13)$$

For F values < 0.85;

$$B(t) = \sqrt{\pi}\sqrt{\pi - \left(\frac{\pi^2 F(t)}{3}\right)} \quad (14)$$

2.4.1.3. Validation of errors for adsorption isotherm and kinetic models. Identifying the most appropriate model for the experimental data obtained from the adsorption technique is a critical step. The coefficient of determination (R^2) alone is insufficient for evaluating the suitability of adsorption models. To determine the most accurate isothermal and kinetic models for Hg^{2+}/Pb^{2+} adsorption on Mag@SAC, a range of error functions was applied.

Normalized standard deviation ($\Delta q\%$, eqn (15)), mean square error (MSE, eqn (16)), hybrid fractional error function (HYBRID, eqn (17)), sum of squares of the errors (SSE, eqn (18)), and chi-square statistic (χ^2, eqn (19)) are the applied error functions.[43–46]

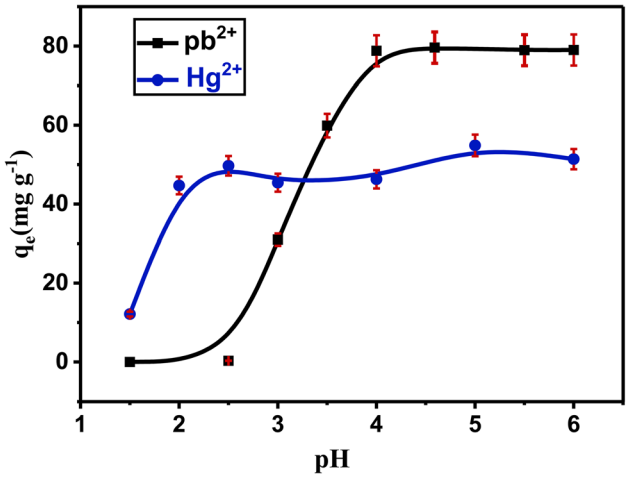

Fig. 8 Effect of pH on Pb^{2+} and Hg^{2+} adsorption on Mag@SAC.

$$\Delta q\% = 100\sqrt{\frac{\sum\left(\frac{q_{e,exp}-q_{e,calc}}{q_{e,exp}}\right)^2}{n-1}} \quad (15)$$

$$\mathrm{MSE} = \frac{1}{n}\sum_{i=1}^{n}\left(q_{e,exp} - q_{e,calc}\right)^2 \quad (16)$$

$$\mathrm{Hybrid} = \frac{100}{N-P}\sum_{i=1}^{n}\left[\frac{\left(q_{e,exp} - q_{e,calc}\right)^2}{q_{e,exp}}\right] \quad (17)$$

$$\mathrm{SSE} = \sum_{i=1}^{n}\left(q_{e,exp} - q_{e,calc}\right)^2 \quad (18)$$

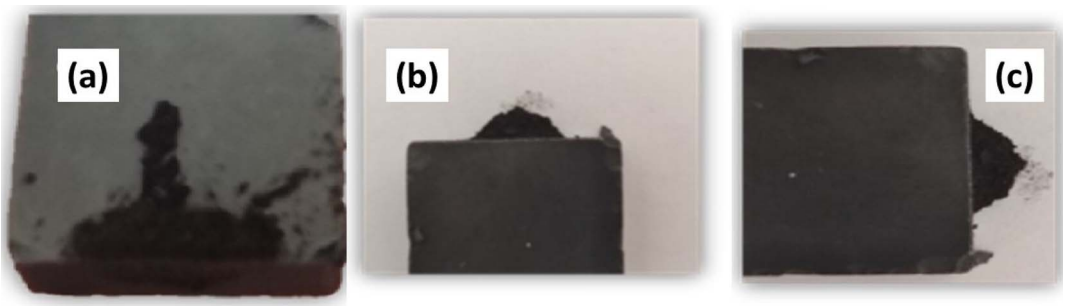

Fig. 7 Digital image (a) Mag@SAC-metal ios dispersed in soluion before application of external magnet; (b) and (c) Mag@SAC-metal ions collected to the surface after the application of an external magnet.

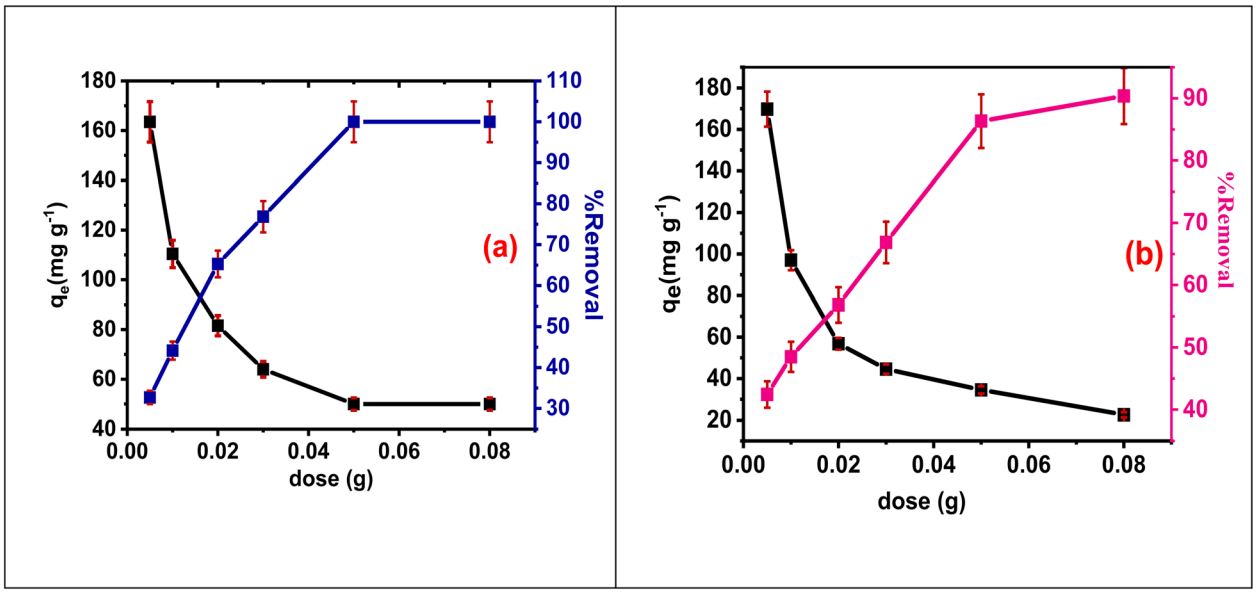

Fig. 9 Effect of adsorbent dosage of Mag@SAC sample for (a) Pb^{2+} and for (b) Hg^{2+} adsorption.

$$\chi^2 = \sum_{i=1}^{n} \frac{\left(q_{e,exp} - q_{e,calc}\right)^2}{q_{e,calc}} \quad (19)$$

$q_{e,exp}$, and $q_{e,calc}$ are amounts actually taken and predicted to be taken, respectively, both are measured in mg g^{-1}. n describes the number of experimental repetitions of the experiment, while p is the number of different settings or factors included in the model.

2.4.1.4. Effect of temperature and thermodynamic studies. Thermodynamic parameters, including standard free energy (ΔG^0_{ads}), enthalpy (ΔH^0_{ads}), and entropy (ΔS^0_{ads}), were determined by examining the temperature influence on the Pb^{2+} and Hg^{2+} adsorption using the Mag@SAC. In the temperature range of 25–60 °C, 0.025 g of Mag@SAC was mixed with 25 mL of 120 mg L^{-1} Pb^{2+} and Hg^{2+} solutions.

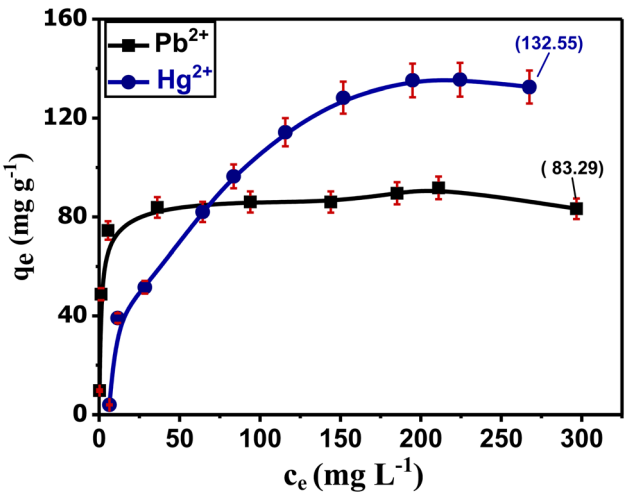

Fig. 10 Effect of initial concentration of Pb^{2+} and Hg^{2+} ions.

The values of enthalpy (ΔH^0_{ads}) and entropy change (ΔS^0_{ads}) were assessed from the slope $\left(\frac{-\Delta H^0_{ads}}{R}\right)$ and the intercept $\left(\frac{\Delta S^0_{ads}}{R}\right)$ from this equation:[47]

$$\ln K_c = \frac{-\Delta H^0_{ads}}{R} + \frac{\Delta S^0_{ads}}{R} \quad (20)$$

R: universal gas constant (8.314×10^{-3} J mol^{-1} K^{-1}) and T: the temperature in (K).

2.5. Desorption studies

A desorption investigation was performed to estimate the Mag@SAC desorption efficiency and potential for reuse. Following adsorption of Pb^{2+} and Hg^{2+} onto Mag@SAC, the material was washed with water to remove unadsorbed metal ions and dried at 105 to 110 °C. Next, 0.025 g of the metal-loaded Mag@SAC was shaken with solutions of varying pH, adjusted from 1.5 to 12 using HCl and NaOH. The solutions were then filtered, and the percentage of Pb^{2+}/Hg^{2+} desorbed was calculated using eqn (21).

$$\text{Desorption\%} = \frac{\text{amount desorped to the solution } (\text{mg L}^{-1})}{\text{amount adsorped to the solution } (\text{mg L}^{-1})} \quad (21)$$

2.6. Analytical applications

Various environmental samples, including distilled water, groundwater, tap water, and various food samples, were utilized to study the removal of Pb^{2+} and Hg^{2+}. Tap water samples were gathered from our lab at Mansoura University in Egypt. All investigated water samples were filtered through a sintered glass G4 filter, then acidified with concentrated nitric acid to pH 2, and stored in polyethylene bottles for further use. One liter of

water sample was mixed with 0.5–1.0 g of $K_2S_2O_8$, and then heated for 30 min at 95 °C, where organic matter is broken down.[48] Then, 0.025 g of Mag@SAC was shaken with varying concentrations of Pb^{2+} and Hg^{2+} from different environmental samples for 60 min, and the mixture was filtered. After reaching equilibrium, the solution was analyzed by atomic absorption spectroscopy to estimate the equilibrium concentrations of Pb^{2+} and Hg^{2+}.

3 Results and discussion

3.1. Materials' design and physicochemical studies

The Mag@SAC biocomposite was synthesized through a two-step process. Initially, SAC biochar was prepared and then steam-activated. In the second step, Fe_3O_4 was impregnated into the SAC to produce the Mag@SAC.

Both SCS and Mag@SAC are black. SCS sample is a very fine, low-density powder and is lighter than the Mag@SAC. In contrast, the newly prepared Mag@SAC is hard, black, and exhibits a more granular texture compared to the SCS. In contrast, the newly prepared biocomposite is hard and exhibits a more granular texture compared to the SCS. To determine solubility, 1 g of Mag@SAC biocomposite was added to 50 mL of water and stirred for 3 hours. After filtration, the solid was carefully dried and weighed, revealing that almost no mass had been lost in the process.

3.1.1. N_2 adsorption–desorption isotherm and BET surface area analysis. Both specific surface area in $m^2\ g^{-1}$ and porosity are critical textural characteristics that influence adsorption capacity, as shown in Fig. 2(a and b) and Table 1. (Mag@SAC) has a high surface area of 417.52 $m^2\ g^{-1}$ and a pore volume of 0.5132 $cm^3\ g^{-1}$, which can exhibit high adsorption capacity for the heavy metals under study. The mean pore diameter of Mag@SAC is 49.17 Å, which falls within the mesoporous range and exceeds the hydrated diameters of Pb^{2+} (8–9 Å) and Hg^{2+} (4.9 Å), thereby facilitating their diffusion into the Mag@SAC pores.

3.1.2. Ash, moisture content, surface pH, point of zero charge, and elemental analysis of the prepared Mag@SAC biocomposite. The surface pH effectively reflects the types of reactive groups present on its surface. At the point of zero charge, in solution, the carbon surface's Brønsted acidic groups frequently donate their protons to water molecules, making the surface negatively charged. Lewis bases, on the other hand,

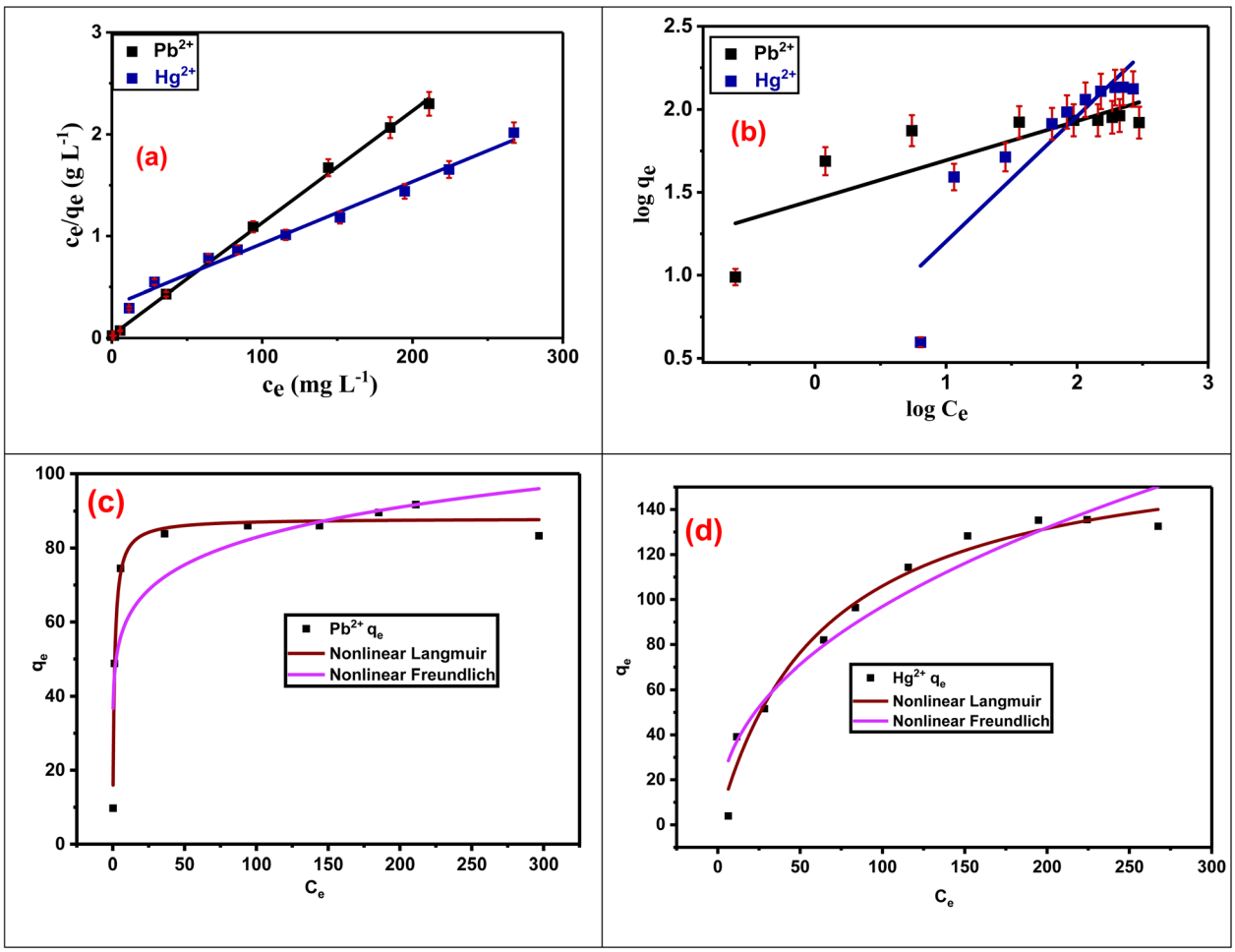

Fig. 11 Adsorption isotherm models: (a) Pb^{2+} and Hg^{2+} linear Langmuir, (b) Pb^{2+} and Hg^{2+} linear Freundlich, (c) Pb^{2+} nonlinear Langmuir and Freundlich, and (d) Hg^{2+} nonlinear Langmuir and Freundlich.

Table 3 Langmuir and the Freundlich isotherm constants for Pb^{2+} and Hg^{2+} ions adsorption

	Mag@SAC sample	Pb^{2+}	Hg^{2+}
Linear Langmuir	q_{m1} (mg g^{-1})	90.82	164.20
	b_1 (L mg^{-1})	0.384	0.019
	R_L	0.0068	0.116
	R^2	0.998	0.984
	χ^2	96.439	437.2
	SSE	8758.638	71 788.25
	MSE	973.182	7178.25
	Hybrid	10 224.097	91 387.963
	$\Delta q\%$	874.359	18 380.836
Linear Freundlich	K_{F1}	28.60	2.80
	$1/n$	0.236	0.755
	R^2	0.657	0.770
	χ^2	165.034	612.219
	SSE	18 088.64	116 579.13
	MSE	2009.84	11 657.913
	Hybrid	16 458.655	126 545.528
	$\Delta q\%$	1338.711	24 924.094
Nonlinear Langmuir	b_2	0.899	0.0157
	q_{m2}	87.97	173.3
	R^2	0.98329	0.9768
	χ^2	89.78	494.95
	SSE	7898.1	85 775.19
Nonlinear Freundlich	K_{F2}	44.37	12.47
	n	7.37	2.25
	R^2	0.75798	0.926
	χ^2	194.55	630.94
	SSE	17 848	121 606

accept protons from the solution, becoming positively charged. Table 2 presents all surface chemical properties of the prepared adsorbent. As shown in Fig. 3, the pH_{PZC} is the pH at which the Mag@SAC's surface charge becomes zero.[44] For the Mag@SAC sample, it equals 6.9, as shown in Table 2. The ash content is slightly high due to the formation of Fe_3O_4, which increases the ash content of the prepared carbon.

3.2. Characterization

3.2.1. Morphology. SEM was used to analyze the surface morphology of both SAC and Mag@SAC. Fig. 4 shows a marked change in activated carbon morphology after modification with nano-magnetite. Steam-activated carbon shows a modest increase in porosity, but after modification with nano-magnetite, it forms well-ordered, small Fe_3O_4 particles.

3.2.2. FTIR spectra. FT-IR spectra of SAC and Mag@SAC samples are displayed in Fig. 5. Both samples exhibit peaks at 3425 and 3429 cm^{-1}, respectively, attributed to O–H stretching vibrations in alcohols, phenols, and adsorbed water in cellulosic materials. Moreover, peaks at 1576–1583 cm^{-1} correspond to the stretching vibrations of C=O bonds in quinone, carboxylic, and ester groups.[49–51] Peaks at 1120–1130 cm^{-1} indicate alcohol (R–OH) groups, while absorption bands at 878 and 880 cm^{-1} are due to (C–H) bending.[51] The SAC sample shows weak bands at 2925–2856 cm^{-1}, attributed to aliphatic (C–H) groups, and a peak at 1384 cm^{-1}, assigned to the in-plane bending vibration of (C–H) in methyl groups.[51–53] In contrast, the SAC/Fe_3O_4 sample is distinguished by a strong band at 612 cm^{-1}, attributed to the Fe–O stretching vibration of Fe_3O_4, confirming the presence of iron nano-magnetite on steam-activated carbon.[54]

3.2.3. Thermo gravimetric analysis (TGA). Fig. 6 demonstrates the TGA result of the Mag@SAC. An initial weight loss (%) of 6.43% between 30 °C and 61 °C is attributed to the release of adsorbed water. A subsequent significant weight loss of 47.26% occurs between 393 °C and 600 °C, likely associated with the decomposition of residual surface functional groups and the dehydrogenation and aromatization of biochar, as supported by FT-IR spectra.[55] Under an inert N_2 atmosphere and in the absence of O_2, magnetite is not expected to undergo oxidation or experience weight gain.

3.2.4. Magnetic property and magnetic separation performance. As reported in the literature, activated carbons possess a small particle size, resulting in a high surface area and significant adsorption efficiency.[56] However, this feature also results in high dispersion and difficulty in separating them from solutions, a major limitation in large-scale applications. This limitation was addressed in the present study by employing the Mag@SAC, which exhibits magnetic properties (Fig. 7). This magnetic property enables efficient separation from solution using an external magnetic field. This property is due to the incorporation of magnetite into the SAC biochar. The separation efficiency of Mag@SAC was evaluated by monitoring its behavior after adsorbing Pb^{2+} and Hg^{2+} metal ions. Initially, Mag@SAC with adsorbed metal ions remained evenly dispersed, producing a turbid suspension. Application of an external magnetic field to the dispersion after adsorption caused the Mag@SAC to migrate toward the magnet and adhere to the container wall, resulting in a clear solution. Upon removal of the external magnetic field, superparamagnetic behavior was observed, and the solution returned to a turbid state. This behavior is due to the Fe_3O_4 magnetic particles present in the biocomposite. It was concluded that the Mag@SAC retains its magnetic properties even after interaction with adsorbed Pb^{2+} and Hg^{2+} metal ions, demonstrating its

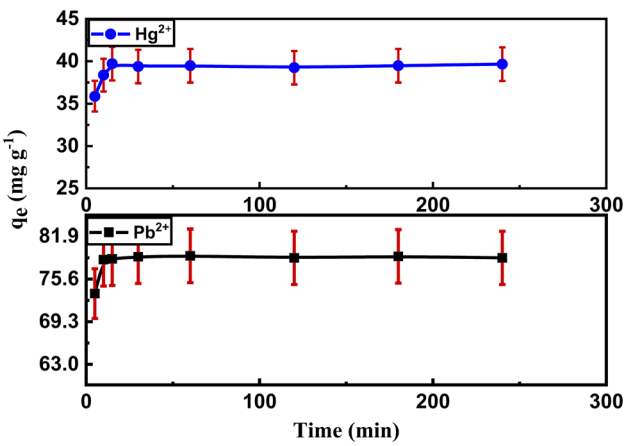

Fig. 12 Effect of contact time on adsorption of Pb^{2+} and Hg^{2+} on Mag@SAC sample.

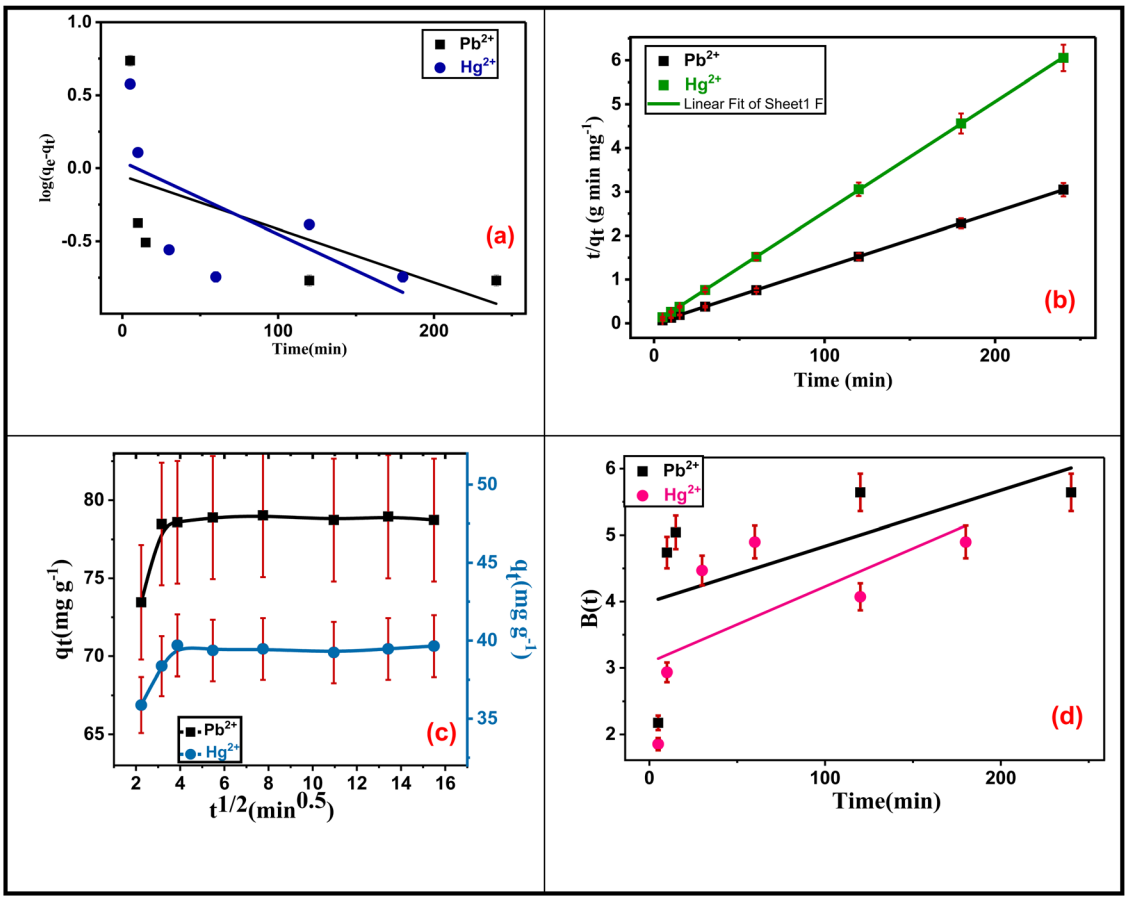

Fig. 13 Kinetic models for adsorption of Pb^{2+} and Hg^{2+}: (a) pseudo-first order, (b) pseudo-second order, (c) intra-particle diffusion, and (d) Boyed model on Mag@SAC activated carbon sample.

structural stability. This indicates the ease with which the current investigation can be applied to large-scale wastewater treatment and reusability. These results agree with those present in the literature.[57,58] This integration of magnetic properties and Mag@SAC functionalities enables advanced, scalable solutions for environmental remediation.

3.3. Adsorption studies

3.3.1. Effect of initial pH on the adsorption of Pb^{2+} and Hg^{2+}. The solution pH affects the surface charge on the activated carbon and the solubility of the metal ions. The pH study of Pb^{2+} and Hg^{2+} adsorption on the Mag@SAC sample was performed by adjusting the pH of the metal solution to 1.5–6. This value was chosen in order to avoid the precipitation of the metal ion in the form of metal hydroxides at higher pH. The pH effect of metal ions adsorption on (Mag@SAC) is graphed in Fig. 8. In the case of Hg^{2+}, the pH increases, giving constant uptake of Hg^{2+} at a pH of 2.5. In the case of Pb^{2+}, the pH increases, and the adsorption of Pb^{2+} remains constant at a pH of 4.5. The influence of pH on Pb^{2+} and Hg^{2+} adsorption by Mag@SAC was investigated over the pH range 1.5–6, which is below Mag@SAC's pH_{PZC}. In this range, adsorption likely occurs primarily through complexation with functional groups rather than solely through surface charge. Moreover, to avoid the precipitation of Hg^{2+} as metal hydroxides at higher pH. The predominant Hg^{2+} species at different pH values are as follows: at pH 2, $HgCl_2$ and $HgCl^+$ account for 88.45%, Hg^{2+} accounts for 3.90%, and HgOHCl accounts for 2%. At pH 4, $Hg(OH)_2$ is the major species at 39.90%, followed by HgOHCl at 25.20%, $HgCl_2$ at 10.02%, with minor proportions of $HgOH^+$, $HgCl^+$, and Hg^{2+} also present. Between pH 6 and 8, $Hg(OH)_2$ (79.62%) and HgOHCl (10.02%) are the predominant species.[16] Niu *et al.* reported that at 100 mg L^{-1} and 20 °C, Pb^{2+} is the predominant species in the pH range of 1.0 to 7.0. They also observed that $Pb(OH)^+$ gradually increases in distribution at pH values above 6.5.[59] The effect of pH on metal ions adsorption on (Mag@SAC) is shown in Fig. 8. For Hg^{2+}, as pH increased from 1.5 to 2.5, adsorption capacity increased, while it remained nearly constant from 2.5 to 6. Pb^{2+} adsorption showed a similar behavior, with minor changes: adsorption capacity increased with pH from 1.5 to 4.5, then remained constant from 4.5 to 6. This may be attributed to the fact that when the solution pH is low, the carbon surface becomes more protonated, leading to a high concentration of H^+ that competes with metal ions for binding sites.[60] As pH increases, reduced protonation and reduced competition with H^+ occur, leading to increased metal ion adsorption.[61]

3.3.2. Effect of adsorbent dose. The amount of Mag@SAC sample influences the removal efficiency of both Pb^{2+} and Hg^{2+}.

Table 4 Kinetic parameters for the adsorption of Pb^{2+} and Hg^{2+}

Model	Parameter	Metal ion Pb^{2+}	Hg^{2+}
PFO	$q_{e,exp}$ (mg g^{-1})	78.73	39.6
	q_{e1} (mg g^{-1})	0.884	1.105
	k_1 (min^{-1})	8.4*10^{-3}	0.011
	R_1^2	0.1453	0.28007
	χ^2	53 996.611	10 349.079
	SSE	47 733.034	11 435.729
	MSE	5966.629	1429.466
	Hybrid	10 179.973	4895.405
	$\Delta q\%$	111.712	107.877
PSO	q_{e2} (mg g^{-1})	78.86	39.61
	k_2 [g mg^{-1} min^{-1}]	0.203	0.0711
	R_2^2	0.999	0.999
	χ^2	0.373	0.3961
	SSE	29.449	15.692
	MSE	3.68	1.961
	Hybrid	6.677	32.962
	$\Delta q\%$	0.0778	0.1715
IPD model	k_{int} [mg(g $min^{1/2}$)]	0.183	0.143
	C	76.68	37.77
	R^2	0.106	0.195
Boyd model	Intercept	3.992	3.0818
	R^2	0.1453	0.28007

This effect was investigated by varying the Mag@SAC dose from 0.005 to 0.08 g. As presented in Fig. 9, the Mag@SAC's adsorption capacity (mg g^{-1}) toward Pb^{2+} and Hg^{2+} decreases as the adsorbent dose (g) increases, while the removal (%) increases. This is attributed to the increased number of available sorption sites and greater surface area that comes with higher Mag@SAC doses, which collectively enhance adsorption (%). However, adsorption efficiency decreases at higher doses due to the presence of unsaturated vacant sites during adsorption.[62–64] From Fig. 9, the maximum removal occurs at an adsorbent dose of 0.05 g for both metal ions, with 100% for Pb^{2+} and 87% for Hg^{2+}.

3.3.3. Effect of initial concentration of heavy metals and adsorption isotherm. The effect of Pb^{2+} and Hg^{2+} concentrations on their removal efficiency by the Mag@SAC was assessed using metal ion concentrations from 5 to 300 mg L^{-1} for Pb^{2+} and 10 to 275 mg L^{-1} for Hg^{2+}, as illustrated in Fig. 10. As illustrated in Fig. 11, the Pb^{2+} and Hg^{2+} concentrations and their removal efficiencies by the Mag@SAC were assessed over the ranges 5–300 mg L^{-1} for Pb^{2+} and 10–275 mg L^{-1} for Hg^{2+}. The adsorption capacity of Mag@SAC for Pb^{2+} and Hg^{2+} ions increased with rising initial metal concentrations, reaching 132.55 mg g^{-1} for Hg^{2+} and 83.29 mg g^{-1} for Pb^{2+}. This increase is attributed to the greater driving force at higher initial Pb^{2+} and Hg^{2+} concentrations, which facilitates overcoming mass-transfer resistance between the metal aqueous solution and Mag@SAC solid phase.[65] The presence of unoccupied metal-binding sites in Mag@SAC further increases the adsorption capacity for Pb^{2+} and Hg^{2+} ions. As these sites become saturated, the adsorption capacity approaches its maximum.[66,67]

It was concluded that the adsorption of the investigated metal ions (Pb^{2+} and Hg^{2+}) onto the Mag@SAC was best described by both linear and nonlinear Langmuir adsorption models. This is supported by higher correlation coefficients (R^2) of (0.998 and 0.983) and (0.984 and 0.9768) for Pb^{2+} and Hg^{2+}, respectively, along with lower Langmuir error function values than those for the Freundlich model, as demonstrated in Table 3. Moreover, from $1/n$ values lower than 1, indicating that the adsorption of Pb^{2+} and Hg^{2+} on Mag@SAC is favored.[68] The R_L values, which indicate the type of isotherm, were calculated to discover if it is irreversible ($R_L = 0$), favorable ($0 < R_L < 1$), linear ($R_L = 1$), or unfavorable ($R_L > 1$).[69] As shown in Table 3, the R_L values for Pb^{2+} and Hg^{2+} range from 0.0068 to 0.166, respectively. These values fall within the range $0 < RL < 1$, indicating that adsorption of Pb^{2+} and Hg^{2+} using the Mag@SAC sample is favored.

3.3.4. Effect of contact time and kinetic studies. Contact time significantly influences the cost of water treatment processes. Accordingly, this study examined the optimal duration required for Pb^{2+} and Hg^{2+} adsorption using Mag@SAC to achieve equilibrium. As presented in Fig. 12, the removal of both Pb^{2+} and Hg^{2+} was measured by varying the oscillation time from 5 to 240 min. Adsorption of Pb^{2+} and Hg^{2+} increased for the first 30 min, then became almost stable after 50 min, reaching equilibrium approximately after 60 min. This trend likely results from the abundance of active sites on the Mag@SAC's surface at higher Pb^{2+} and Hg^{2+} concentrations during the initial phase. By increasing the oscillating time by more than 60 min, the Mag@SAC adsorption capacity became constant, and the Pb^{2+} and Hg^{2+} adsorption attained equilibrium. Therefore, 60 min of oscillation time is chosen as the adsorption time for the experimental test to ensure equilibrium is reached.[66]

Several kinetic models were investigated to evaluate the best-fitting model, including the PFO, PSO, and IPD, as well as the Boyd model, as shown in Fig. 13 and Table 4. It was observed that PSO is a better-fitting model, with higher R^2 values (0.999) and lower error metrics ($\Delta q\%$, χ^2, SSE, MSE, and hybrid) than

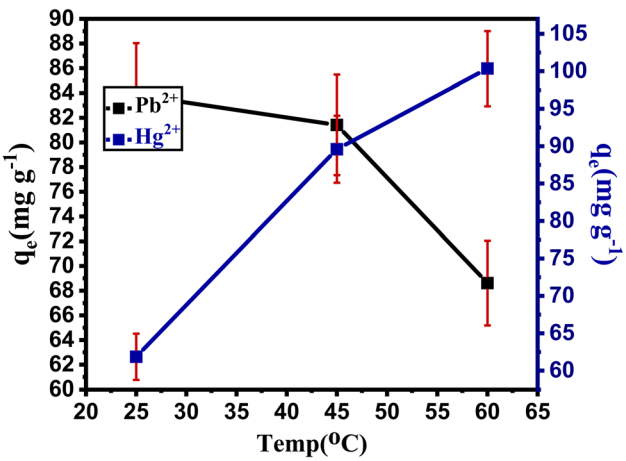

Fig. 14 Effect of temperature on Pb^{2+} and Hg^{2+} adsorption using Mag@SAC.

Table 5 Thermodynamic parameters for the adsorption of Pb^{2+} and Hg^{2+} on Mag@SAC

	Metal ions					
Parameter	Pb^{2+}			Hg^{2+}		
T (k)	298.15	318.15K	333.15	298.15	318.15	333.15
ΔG^0 (kJ mol^{-1})	−2.085	−1.976	−0.8019	−0.153	−2.857	−4.516
ΔH^0 (kJ mol^{-1})	−12.296			37.25		
ΔS^0 (J mol^{-1} k^{-1})	−33.72			125.64		

PFO for the two investigated contaminants. Additionally, the equilibrium adsorption capacity (q_e) values predicted by the PSO model closely align with the $q_{e,exp}$. Kinetic studies indicate that the PSO mechanism best represents the adsorption of Pb^{2+} and Hg^{2+} by the Mag@SAC biocomposite. For the IPD, in some cases, both film diffusion and intraparticle diffusion influence adsorption kinetics. In many adsorption processes, solute uptake varies almost proportionally with $t^{1/2}$ rather than contact time t.[70] In this study, the q_t *versus* $t^{1/2}$ plot does not pass through the origin (Fig. 13c), indicating that IPD is not the sole rate-limiting step and that boundary-film diffusion also contributes to sorption.[40,71] As presented in Fig. 13d, the linear plots of the Boyd model do not go through the origin, indicating that boundary-layer diffusion plays a significant role alongside other mechanisms in the sorption process.

3.3.5. Effect of temperature and thermodynamic studies. Temperature significantly influences heavy metal removal by adsorbents, and the optimal temperature depends on both the adsorbent and adsorbate. As the temperature elevated, the q_e of the Mag@SAC increased for Hg^{2+} and decreased for Pb^{2+}, as presented in Fig. 14.

The thermodynamic parameters, $\Delta G ads^0$, ΔH^0_{ads}, and ΔS^0_{ads}, associated with the adsorption of Pb^{2+} and Hg^{2+} onto Mag@SAC were determined, and the data tabulated in Table 5. As demonstrated in Table 5 and Fig. 15, the negative ΔG^0_{ads} values for both Pb^{2+} and Hg^{2+} indicate that their adsorption on Mag@SAC is thermodynamically feasible and spontaneous. For Pb^{2+} adsorption, the negative values of ΔH^0_{ads} and ΔS^0_{ads} indicate an exothermic process and decreased randomness at the solid-solution interface, resulting in lower system randomness and greater alignment.[72,73] For Hg^{2+} adsorption, positive values of ΔH^0_{ads} and ΔS^0_{ads} indicate endothermic adsorption onto the Mag@SAC and increased randomness at the adsorbent–adsorbate interface, respectively.[74,75]

3.3.6. Effect of ionic strength. The effect of ionic strength on Pb^{2+} and Hg^{2+} adsorption using the Mag@SAC sample is shown in Fig. 16. The adsorption was examined by removing 20 mg L^{-1} of Pb^{2+} and Hg^{2+} without pH adjustment to avoid interference from the buffer ions. Fig. 16 illustrates that for Pb^{2+} ions, there is no significant influence of the coexisting ions on their removal process. For Hg^{2+} ions, however, increasing the solution's ionic strength from 0.001 to 0.15 mole per L leads to a noticeable drop in removal efficiency, falling from 97.3% at the lowest concentration to 91% at 0.08 mole per L. This decline in removal efficiency likely results from competition between

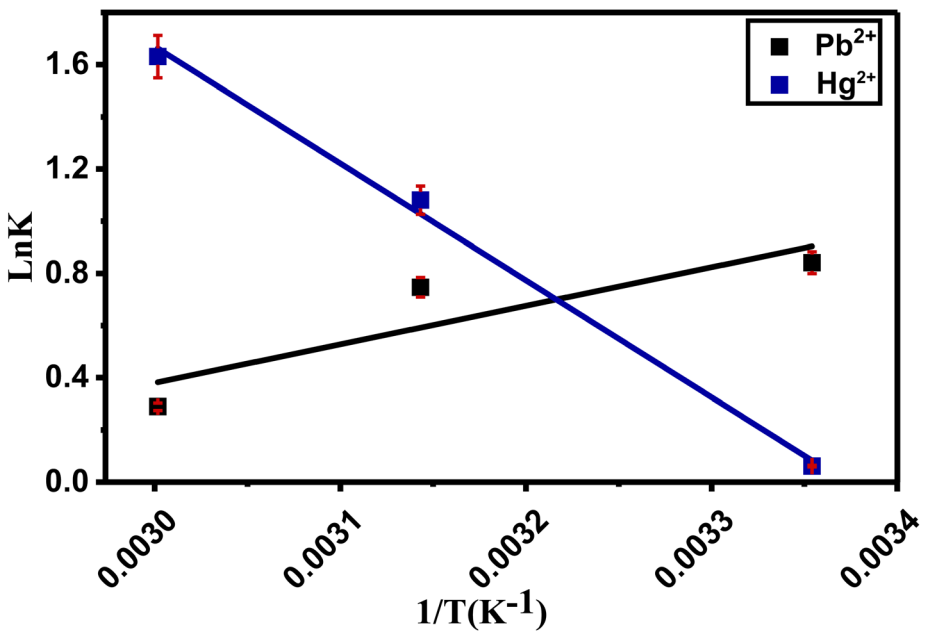

Fig. 15 Plot of $1/T$ *vs.* ln K for adsorption of Pb^{2+} and Hg^{2+} on the Mag@SAC sample.

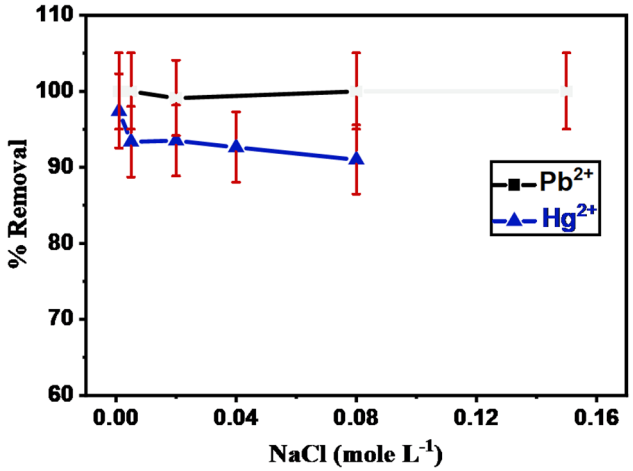

Fig. 16 Effect of ionic strength on adsorption of Pb^{2+} and Hg^{2+} on Mag@SAC sample.

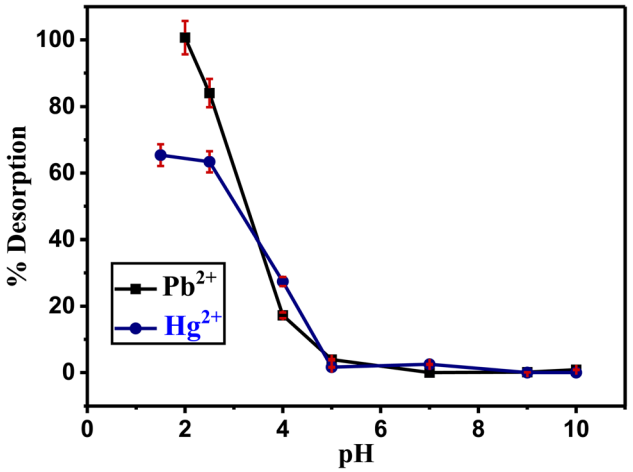

Fig. 17 Effect of pH on the % desorption Mag@SAC.

Hg^{2+} ions and sodium cations for the available adsorption sites. Overall, the removal of these metal ions remains only slightly influenced by changes in water ionic strength.

3.3.7. Effect of foreign ions. The actual matrix present in water (anions and cations) may influence the removal of heavy metal ions. The removal efficiency of 20 mg L^{-1} Pb^{2+} and Hg^{2+} was measured in the presence of 100 mg L^{-1} of matrices such as fluoride, oxalate, acetate, Ca^{2+}, KH_4^+, and Mg^{2+}. The obtained data are tabulated in Table 6. It was concluded that the adsorption of Pb^{2+} and Hg^{2+} is slightly affected by the presence of these matrices, with removal ranging from 99.7% to 91.5%. Only the Mg^{2+} cation can affect heavy metal ion removal by increasing water hardness, thereby altering the removal process.

3.3.8. Desorption studies. The regenerative capacity of the Mag@SAC sample is a useful indicator of its commercial potential.[76] Chemical treatments are typically employed as the primary method for regenerating exhausted adsorbents. This study examined how pH affects Mag@SAC recovery after Pb^{2+} and Hg^{2+} removal using NaOH and HCl. After that, the loaded Mag@SAC-metal ion is filtered and dried in an oven for further use. The loaded adsorbent is then immersed in solutions at different pH values (1.5–10) to study the % desorption efficiency. From Fig. 17, we can see that for Pb^{2+}, the desorption efficiency reaches 100% at pH 2 and decreases as the solution pH increases. For Hg^{2+}, the desorption efficiency reaches 65.38% at pH 1.5 and decreases as the solution pH increases. From these results, we can use this adsorbent several times, as the desorption efficiency is high.

Table 6 Effect of foreign ions' presence on the removal of Pb^{2+} and Hg^{2+} using Mag@SAC

	Metal ions	
	% removal efficiency	
Foreign ions (100 mg L^{-1})	Pb^{2+}	Hg^{2+}
Acetate	99.45	92.00
Cl	99.72	97.96
F	97.66	92.87
PO_4^{3-}	95.74	96.94
NH_4^+	98.07	97.38
Na^+	99.03	91.42
Ba^{2+}	99.58	94.47
Mg^{2+}	—	69.04

3.3.9. Analytical applications. The potential of Mag@SAC for the adsorption of Pb^{2+} and Hg^{2+} from various environmental samples, including distilled water, tap water, ground water, and digested food samples, was evaluated. 0.025 g of the adsorbent and 25 mL of the aforementioned environmental samples were placed in PVC flasks, together with 20 mg L^{-1} of Pb^{2+} and Hg^{2+} spiked. A study was done on the filtrate. The gathered information is depicted in Table 7.

3.3.10. Plausible mechanism of adsorption of Pb^{2+} and Hg^{2+} onto Mag@SAC biocomposite. To investigate the possible mechanisms of Hg^{2+} and Pb^{2+} adsorption on the Mag@SAC, isotherms, kinetics, thermodynamics, and FTIR spectra before and after adsorption were assessed.

3.3.11. FT-IR. Fig. 18 presents the FTIR spectra of the Mag@SAC before and after adsorption of Pb^{2+} and Hg^{2+}. Changes in the absorption peaks indicate the adsorption of these heavy metals. Following adsorption, the O–H peak at 3425 cm^{-1} shifts to 3444 cm^{-1} for Pb^{2+} and 3451 cm^{-1} for Hg^{2+}. The peak at 1576 cm^{-1}, attributed to C=O, shifts to 1628 cm^{-1} for both metals. The C–H peak at 1341 cm^{-1} shifts to 1385 cm^{-1} for Pb^{2+} and 1388 cm^{-1} for Hg^{2+}. The F–O peak at 612 cm^{-1} shifts to lower wavenumbers.

Pb^{2+} and Hg^{2+} adsorption on the Mag@SAC occurs mainly through surface complexation, with electrostatic attraction further enhancing the process. FTIR spectral shifts (Fig. 18), pH-dependent adsorption studies (Fig. 8), and literature support these findings. Incorporating Fe_3O_4 into SAC biochar increases adsorption capacity by expanding surface area and introducing more active groups. Fe_3O_4 provides a high specific surface area and numerous active sites for chemical bonding. Biochar contributes active groups, including –OH and –COOH, which facilitate effective cation binding.

Table 7 Recovery of Pb^{2+} and Hg^{2+} metal ions from different environmental samples using Mag@SAC sample ($n = 3$)

		Pb^{2+}		Hg^{2+}	
Environmental samples	Metal ions, mg L^{-1}	Recovery (R, %)	RSD	Recovery (R, %)	RSD
Deionized water	0	—	—	—	—
	10	97.5	1.14	94	0.81
	15	96	0.7	88.5	1.17
	20	91.85	1.3	70.05	1.1
Tap water	0	—	—	—	—
	10	100	0.21	95.85	0.64
	15	100	0.14	91.92	0.43
	20	100	0.08	85.41	1.3
Ground water	0	—	—	—	—
	10	100	0.31	94.65	1.32
	15	100	0.4	92.125	1
	20	100	0.12	85.8	1.8
Herbal extract	10	58.56	1.9	—	—
	20	52.93	1.74	—	—
Cauliflower	10	—	—	89.21	0.94
	20	—	—	83.6	1.11
Flour	10	—	—	21.6	1.23
	20	1.73	0.12	33.55	0.39

Surface complexation binds Pb^{2+} or Hg^{2+} ions to oxygen-containing functional groups on Mag@SAC,[77] while electrostatic attraction also supports adsorption. Solution pH influences the ionization of surface groups on biochar-derived materials. Exceeding the pH_{PZC}, the Mag@SAC surface becomes negatively charged, attracting metal ions. At lower pH, excess H^+ ions compete for binding sites, reducing adsorption efficiency.[78] At higher pH, deprotonation of carboxyl and hydroxyl groups increases electrostatic attraction and improves metal ion binding.[79]

Additional mechanisms, such as ion exchange and pore-filling, also contribute to metal ion adsorption on magnetite-supported composites. Iron oxide-modified biochar exhibits strong ion-exchange capacity, helping immobilize toxic metals over time.[80] Through ion exchange, these composites capture metal ions and convert them into less mobile, more stable forms. The combined effects of surface complexation and ion exchange offer an effective dual mechanism for long-term heavy-metal containment.

The suggested mechanism of the removal of Pb^{2+} and Hg^{2+} ions using Mag@SAC is shown in Fig. 19.

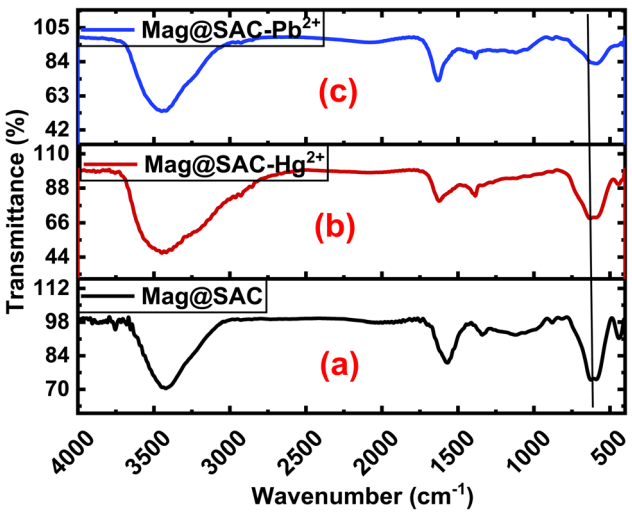

Fig. 18 FTIR spectra of (a) Mag@SAC, (b) Mag@SAC-Hg^{2+}, and (c) Mag@SAC-Pb^{2+}.

3.4. Performance of the Mag@SAC biocomposite

To evaluate the Mag@SAC value, a comparison of Mag@SAC q_e with other reported adsorbents for Pb^{2+} and Hg^{2+} removal was conducted, as presented in Table 8. It was observed that Pb^{2+} and Hg^{2+} adsorption by Mag@SAC is reasonably comparable to other investigations, with q_e values of 83.29 and 132.55 mg g^{-1}, respectively, and higher than those reported for other materials.

3.5. Future recommendations

Functionalized magnetite-biochar biocomposites offer an effective and versatile solution for large-scale wastewater treatment and the adsorption of hazardous metals such as Pb^{2+} and Hg^{2+}. By combining the high adsorption capacity of biochar with the magnetic properties of magnetite, these composites emerge as promising alternatives to conventional treatment methods and as viable candidates for future environmental remediation.

Magnetic separation enables rapid, efficient removal and reuse of Mag@SAC, reducing operational complexity and costs in industrial and municipal applications by streamlining separation processes, which is essential for large-scale operations.[91] Furthermore, the porous structure of biochar and its surface functional groups, such as carboxyl and hydroxyl groups, facilitate strong interactions with metal ions, thereby

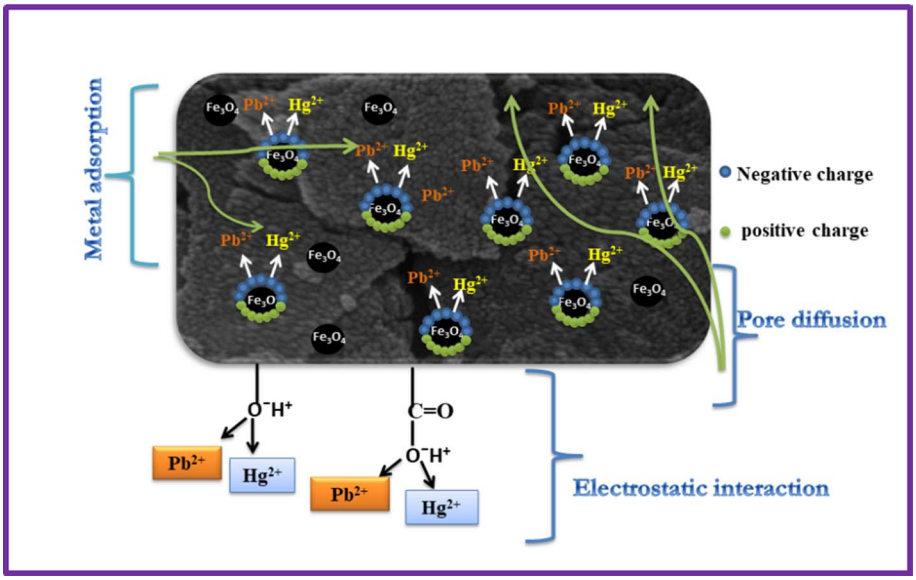

Fig. 19 Plausible mechanism of adsorption of Pb^{2+} and Hg^{2+} on Mag@SAC.

enhancing the adsorption of toxic metals even at low concentrations.[92]

Scaling up these composites poses challenges, including maintaining adsorption efficiency at higher metal concentrations and ensuring stability across varying pH conditions. Advanced modifications, including amino-functionalized magnetic biochars and structural adjustments, have improved stability and performance in diverse environments.[93] However, further optimization is necessary to achieve consistent efficacy in real wastewater systems, which often contain mixed metal ions and organic compounds that can impede adsorption. Stability is particularly important in acidic wastewater, where the durability of magnetite particles and the preservation of biochar's functional groups affect adsorption rates and metal-binding efficiency.[94]

Regeneration and reuse are essential for the large-scale application of these composites. Studies demonstrate that magnetite-biochar composites can be regenerated by simple washing or chemical treatments, enabling multiple cycles of heavy metal removal without significant loss of adsorption capacity.[95] This regenerative property lowers long-term operational costs and reduces environmental impact by decreasing the frequency of adsorbent replacement, thereby supporting both economic and life-cycle sustainability.[91]

By supporting sustainability and resource recovery, this hybrid system provides an effective treatment solution and promotes environmental stewardship through waste valorization and circular economy practices. As research and technology continue to evolve, magnetite-modified biochar composites such as Mag@SAC are poised to revolutionize large-scale wastewater treatment, driving greater efficiency, adaptability, and sustainability.

3.6. Alignment with sustainable development goals

In conclusion, this approach supports multiple sustainable development goals by addressing critical challenges in environmental sustainability and resource efficiency. The current investigation demonstrates the transformation of waste into innovative materials that align with SDGs 6, 12, 13, and 15,

Table 8 Comparison of the maximum sorption capacity of Pb^{2+} and Hg^{2+} by different biosorbents

Adsorbent	Hg^{2+} q_e (mg g^{-1})	Pb^{2+} q_e (mg g^{-1})	Ref.
Peel biomass of Pachira aquatic Aubl	0.71	—	81
Rhodamine hydrazide-modifying Fe_3O_4 microspheres	7.5	—	82
Coal fly ash	0.44	—	83
Activated carbon from mango kernel	19.762	—	84
Palm shell powder 6	7.134	—	85
Raw CNT	—	1.66	86
Thiol-functionalized cellulosic biomass	—	28.67	87
Copolymer 2-hydroxyethyl acrylate with monomer methyl methacrylate (MMA-HEMA)	—	31.447	88
H_2SO_4-treated CNS	—	8.73	89
Plum kernel	—	1.3	90
Magnetic activated carbon derived from SB	132.55	83.29	Present study

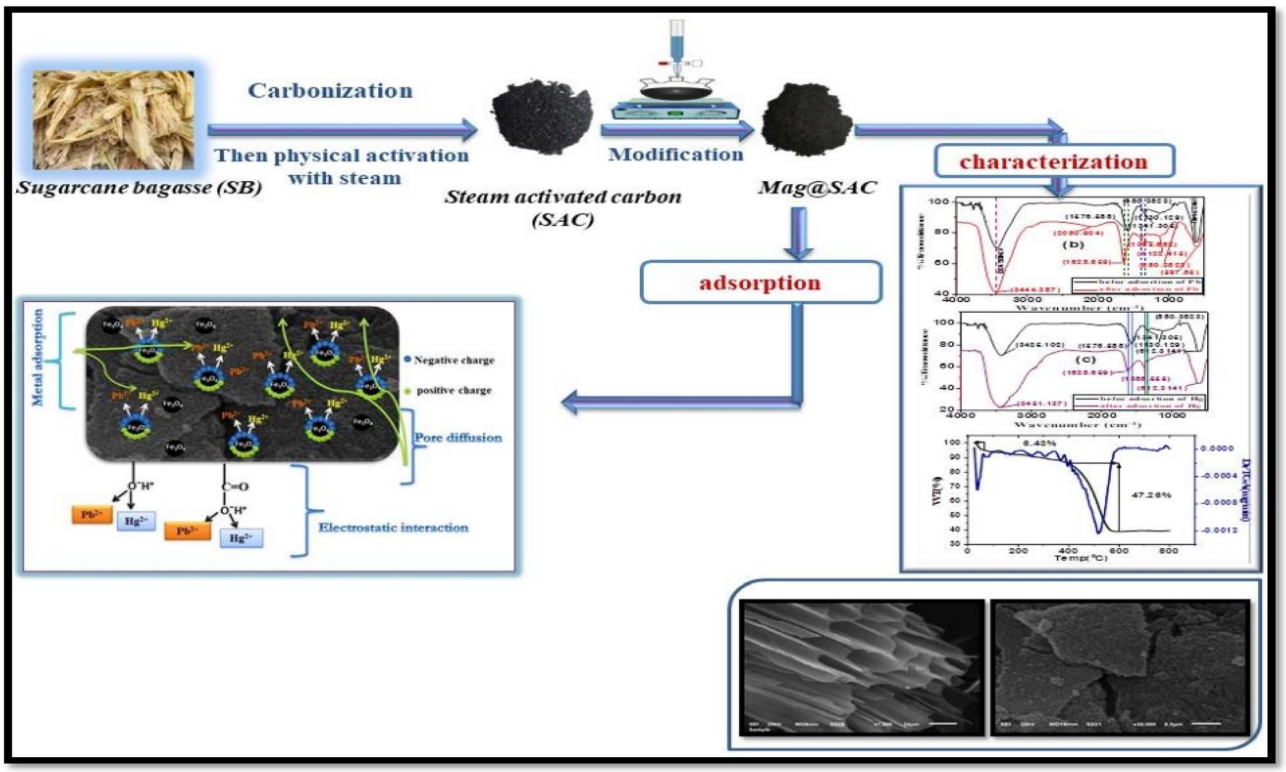

Fig. 20 Graphical representation of the synthesis, characterization, and mechanism of the adsorption of Pb^{2+} and Hg^{2+} ions onto Mag@SAC.

thereby making acid mine drainage treatment more affordable and effective while protecting water quality and supply.

3.7. Limitations

To improve this technology's applicability, key limitations must be addressed. These include the composite's stability in extreme pH and high metal concentrations, potential biochar degradation over time, and the impact of co-contaminants in actual wastewater. Further research is also required to evaluate the system's long-term economic feasibility and scalability, especially regarding material synthesis costs and maintenance.

4 Conclusion

Mag@SAC functions as a novel, environmentally friendly biosorbent for the removal of Pb^{2+} and Hg^{2+} from diverse water and food samples, achieving maximum q_e values of 83 and 132 mg g^{-1}, respectively, within 60 minutes. Analyses of adsorption isotherms and kinetics reveal that Pb^{2+} and Hg^{2+} follow the Langmuir and PSO models most closely, offering clear insight into their distinct adsorption behaviors. Thermodynamic studies show that Pb^{2+} adsorption is exothermic, while Hg^{2+} adsorption is endothermic. Desorption experiments indicate that Mag@SAC can be economically reused, with desorption efficiencies ranging from 70% to 100% at low pH. These findings confirm the effectiveness of Mag@SAC as an adsorbent for metal ion removal in diverse environmental contexts, attributed to the synergistic adsorption properties of magnetite-biochar. The system offers operational flexibility, supports environmental sustainability, and facilitates regeneration and reuse, making it a viable alternative to conventional heavy-metal treatment methods.

Fig. 20 presents the synthesis, characterization, and adsorption mechanism of Pb^{2+} and Hg^{2+} on Mag@SAC.

Ethical approval

Not applicable to this study.

Consent for publication

Not applicable to this study.

Author contributions

Magda A. Akl: conceptualization, methodology, investigation, writing – original draft, review, supervision, Aya G. Mostafa: methodology, investigation, writing – original draft, review, Asmaa A. Serag: methodology, investigation, writing – original draft, review.

Conflicts of interest

The authors declare that they have no competing interests.

Data availability

The authors declare that the data supporting the findings of this study are available within the paper and its supplementary information (SI) files.

Supplementary information is available. See DOI: https://doi.org/10.1039/d6ra03304k.

Acknowledgements

Not applicable to this study.

References

1 A. Alam, A. Hassan, Z. Sultana and N. Das, Natural polymer-based bioadsorbents for wastewater treatment, *RSC Sustainability*, 2025, **3**, 5027–5050.
2 K. F. Kayani and S. J. Mohammed, Heavy metal pollution in aquatic environments and removal using highly efficient bimetallic metal–organic framework adsorbents, *RSC Adv.*, 2025, **15**(43), 35756–35769.
3 S. Meftah, K. Meftah, M. Drissi, I. Radah, K. Malous, A. Amahrous, A. Chahid, T. Tamri, A. Rayyad, B. Darkaoui and S. Hanine, Heavy metal polluted water: Effects and sustainable treatment solutions using bio-adsorbents aligned with the SDGs, *Discover Sustain.*, 2025, **6**(1), 137.
4 K. H. Aziz, F. S. Mustafa, K. M. Omer, S. Hama, R. F. Hamarawf and K. O. Rahman, Heavy metal pollution in the aquatic environment: efficient and low-cost removal approaches to eliminate their toxicity: a review, *RSC Adv.*, 2023, **13**(26), 17595–17610.
5 M. Balali-Mood, K. Naseri, Z. Tahergorabi, M. R. Khazdair and M. Sadeghi, Toxic mechanisms of five heavy metals: mercury, lead, chromium, cadmium, and arsenic, *Front. Pharmacol.*, 2021, **12**, 643972.
6 M. Durkalec, M. Martínez-Haro, A. Nawrocka, J. Pareja-Carrera, J. E. Smits and R. Mateo, Factors influencing lead, mercury and other trace element exposure in birds from metal mining areas, *Environ. Res.*, 2022, **212**, 113575.
7 R. Roy, S. Samanta, S. Pandit, T. Naaz, S. Banerjee, J. M. Rawat, K. K. Chaubey and R. P. Saha, An overview of bacteria-mediated heavy metal bioremediation strategies, *Appl. Biochem. Biotechnol.*, 2024, **196**(3), 1712–1751.
8 F. Kriswandana and W. Winarko, The Effectiveness of Reduction of Weight Metal Contents of Pb, and Hg in Water Electro-coagulation Method, *J. Global Pharma Technol.*, 2020, 306–313.
9 Q. Chen, Y. Yao, X. Li, J. Lu, J. Zhou and Z. Huang, Comparison of heavy metal removals from aqueous solutions by chemical precipitation and characteristics of precipitates, *J. Water Process Eng.*, 2018, **26**, 289–300.
10 H. Zeng, L. Wang, D. Zhang and C. Wang, Efficient capture and detoxification of mercury dichloride from wastewater by a PVDF/PEI adsorption membrane, *Chem. Eng. J.*, 2023, **468**, 143621.
11 M. A. Akl, N. A. El-Mahdy and E. S. El-Gharkawy, Design, structural, spectral, DFT and analytical studies of novel nano-palladium schiff base complex, *Sci. Rep.*, 2022, **12**(1), 17451.
12 Y. Huang, Q. Dong, X. Yu, R. Huang, Y. Han, X. Zeng, X. Luo, X. Fan, H. Li, J. Qin and R. Wang, Recovering metallic lead from spent lead paste by slurry electrolysis, *Sep. Purif. Technol.*, 2025, **354**, 128789.
13 J. M. López-Jiménez, P. A. Alvizuri-Tintaya, G. A. Chávez-Lizárraga, V. G. Lo-Iacono-Ferreira, J. I. Torregrosa-López and J. Lora-García, Lead Removal by Reverse Osmosis: Seeking Sustainability in the Operation of Advanced Technologies: A Preliminary Study, *Sustainability*, 2025, **17**(16), 7270.
14 E. Sgreccia, C. Rogalska, F. S. Gallardo Gonzalez, P. Prosposito, L. Burratti, P. Knauth and M. L. Di Vona, Heavy metal decontamination by ion exchange polymers for water purification: counterintuitive cation removal by an anion exchange polymer, *J. Mater. Sci.*, 2024, **59**(7), 2776–2787.
15 M. MH Al-Awadhi, M. Bashnaini and M. A. Akl, Biosorption of Lead (II) and Aluminum (III) from real water samples onto precursor pistachio shells: Adsorption characteristics, kinetics and thermodynamic studies, *Egypt. J. Chem.*, 2023, **66**(10), 259–268.
16 M. A. Akl and A. G. Mostafa, Novel aminothiazole grafted cellulose composite for efficient removal of Hg(II) from wastewater in single and multicomponent systems, *Sci. Rep.*, 2025, **15**, 45673.
17 A. S. Mahmouda, N. A. Youssefa, A. O. Abo El Nagab and M. M. Selimc, Removal of copper ions from wastewater using magnetite loaded on active carbon (AC) and oxidized active carbon (OAC) Support, *J. Sci. Res. Sci.*, 2019, **36**(1), 226–247.
18 G. Athira, A. Bahurudeen and V. S. Vishnu, Availability and accessibility of sugarcane bagasse ash for its utilization in Indian cement plants: A GIS-based network analysis, *Sugar Technol.*, 2020, **22**(6), 1038–1056.
19 S. M. Kakom, N. M. Abdelmonem, I. M. Ismail and A. A. Refaat, Activated carbon from sugarcane bagasse pyrolysis for heavy metals adsorption, *Sugar Technol.*, 2023, **25**(3), 619–629.
20 N. M. Msimango, F. M. Makhanya, P. Ntola and L. Q. Qwabe, Remediation of Ni (II) using sugarcane bagasse and its chemically modified derivatives: A comparison of linear and non-linear kinetic and isotherm models, *Sep. Sci. Technol.*, 2025, **60**(7), 899–917.
21 D. M. Sandrini, D. P. Fuentes, P. V. Oliveira and D. F. Petri, Sugarcane bagasse/kapok fiber-based filters for simultaneous demulsification and removal of Li+ ions from the waste of lithium grease production, *Sep. Purif. Technol.*, 2025, **361**, 131484.
22 M. Namdeo, Magnetite nanoparticles as effective adsorbent for water purification-a review, *Advances in Recycling & Waste Management*, 2018, **2**(3), 126–129.
23 M. N. Kayes, M. M. Chowdhury, M. A. Seikh, M. H. Suhag and F. Akter, Application of sugarcane bagasse as an adsorbent for treatment of a textile dye Rhodamine B, *Barishal Univ. J. Part 1*, 2019, **6**, 47–57.
24 E. S. Abd, A. El-Maghraby and N. Taha, Adsorption studies of cationic dye on raw and modified sugarcane bagasse from aqueous solutions: Kinetic and isotherm aspects, *Egypt. J. Chem.*, 2021, **64**(3), 1593–1600.

25 M. A. Akl and A. A. Serage, Chitosan impregnated sugarcane bagasse biochar for removal of anionic dyes from wastewater, *Sci. Rep.*, 2024, **14**(1), 27097.
26 A. I. Abd-Elhamid, A. G. Mostafa, A. A. Nayl and M. A. Akl, Novel sulfonic groups grafted sugarcane bagasse biosorbent for efficient removal of cationic dyes from wastewater, *Sci. Rep.*, 2024, **14**(1), 19129.
27 I. Lestari, E. Kurniawan, D. R. Gusti and Yusnelti, Magnetite Fe3O4-activated carbon composite as adsorbent of rhodamine B dye, in *IOP Conference Series: Earth and Environmental Science*, IOP Publishing, 2020, vol. 483, iss 1, p. 012046.
28 S. Brunauer, P. H. Emmett and E. Teller, Adsorption of gases in multimolecular layers, *J. Am. Chem. Soc.*, 1938, **60**(2), 309–319.
29 I. D. Smičiklas, S. K. Milonjić, P. Pfendt and S. Raičević, The point of zero charge and sorption of cadmium (II) and strontium (II) ions on synthetic hydroxyapatite, *Sep. Purif. Technol.*, 2000, **18**(3), 185–194.
30 S. Singh, A. Dzeranov, L. Bondarenko, K. Kydralieva, G. Dzhardimalieva, A. Babaytsev, G. Kugabaeva, N. Golubeva and B. C. Yadav, Modified Fe3O4 magnetite Core@ Shell type nanomaterials for highly-responsive LPG sensing: a comparative analysis, *ECS Sens. Plus*, 2023, **2**(1), 013601.
31 A. Örnek, M. Özacar and İ. A. Şengil, Adsorption of lead onto formaldehyde or sulphuric acid treated acorn waste: equilibrium and kinetic studies, *Biochem. Eng. J.*, 2007, **37**(2), 192–200.
32 N. K. Amin, Removal of reactive dye from aqueous solutions by adsorption onto activated carbons prepared from sugarcane bagasse pith, *Desalination*, 2008, **223**(1–3), 152–161.
33 M. A. Al-Ghouti, D. Da'ana, M. Abu-Dieyeh and M. Khraisheh, Adsorptive removal of mercury from water by adsorbents derived from date pits, *Sci. Rep.*, 2019, **9**(1), 15327.
34 S. Karagöz, T. Tay, S. Ucar and M. Erdem, Activated carbons from waste biomass by sulfuric acid activation and their use on methylene blue adsorption, *Bioresour. Technol.*, 2008, **99**(14), 6214–6222.
35 F. Haghseresht and G. Q. Lu, Adsorption characteristics of phenolic compounds onto coal-reject-derived adsorbents, *Energy Fuels*, 1998, **12**(6), 1100–1107.
36 P. K. Khare, *Treatment of phenolic water using adsorption*, Doctoral dissertation, Department of Chemical Engineering, National Institute of Technology Rourkela, Rourkela, 2011.
37 M. T. Amin, A. A. Alazba and M. Shafiq, Effective adsorption of methylene blue dye using activated carbon developed from the rosemary plant: isotherms and kinetic studies, *Desalin. Water Treat.*, 2017, **74**, 336–345.
38 H. Yuh-Shan, Citation review of Lagergren kinetic rate equation on adsorption reactions, *Scientometrics*, 2004, **59**(1), 171–177.
39 V. C. Srivastava, M. M. Swamy, I. D. Mall, B. Prasad and I. M. Mishra, Adsorptive removal of phenol by bagasse fly ash and activated carbon: equilibrium, kinetics and thermodynamics, *Colloids Surf., A*, 2006, **272**(1–2), 89–104.
40 A. Khaled, A. El Nemr, A. El-Sikaily and O. Abdelwahab, Removal of Direct N Blue-106 from artificial textile dye effluent using activated carbon from orange peel: adsorption isotherm and kinetic studies, *J. Hazard. Mater.*, 2009, **165**(1–3), 100–110.
41 G. E. Boyd, A. W. Adamson and Jr L. S. Myers, The exchange adsorption of ions from aqueous solutions by organic zeolites. II. Kinetics1, *J. Am. Chem. Soc.*, 1947, **69**(11), 2836–2848.
42 D. Reichenberg, Properties of ion-exchange resins in relation to their structure. III. Kinetics of exchange, *J. Am. Chem. Soc.*, 1953, **75**(3), 589–597.
43 C. R. Girish and V. Ramachandramurty, Kinetic Studies on Removal of Phenolic Compounds from Wastewater Using Agricultural Waste: A Review, *J. Environ. Sci. Eng.*, 2016, **58**(2), 147–158.
44 Y. F. Jia, B. Xiao and K. M. Thomas, Adsorption of metal ions on nitrogen surface functional groups in activated carbons, *Langmuir*, 2002, **18**(2), 470–478.
45 L. T. Popoola, Characterization and adsorptive behaviour of snail shell-rice husk (SS-RH) calcined particles (CPs) towards cationic dye, *Heliyon*, 2019, **5**(1), e01153.
46 S. M. Miraboutalebi, S. K. Nikouzad, M. Peydayesh, N. Allahgholi, L. Vafajoo and G. McKay, Methylene blue adsorption via maize silk powder: Kinetic, equilibrium, thermodynamic studies and residual error analysis, *Process Saf. Environ. Prot.*, 2017, **106**, 191–202.
47 D. D. Duong, *Adsorption Analysis: Equilibria and Kinetics*, Imperial College Press, London, 1998.
48 M. A. Akl, M. B. Dawy and A. A. Serage, Efficient removal of phenol from water samples using sugarcane bagasse based activated carbon, *J. Anal. Bioanal. Tech.*, 2014, **5**(2), 1–2.
49 A. Macías-García, M. A. Díaz-Díez, E. M. Cuerda-Correa, M. Olivares-Marin and J. Ganan-Gomez, Study of the pore size distribution and fractal dimension of HNO3-treated activated carbons, *Appl. Surf. Sci.*, 2006, **252**(17), 5972–5975.
50 H. Marsh and F. R. Reinoso, *Activated Carbon*, Elsevier, 2006.
51 T. Yang and A. C. Lua, Textural and chemical properties of zinc chloride activated carbons prepared from pistachio-nut shells, *Mater. Chem. Phys.*, 2006, **100**(2–3), 438–444.
52 T. H. Liou, Development of mesoporous structure and high adsorption capacity of biomass-based activated carbon by phosphoric acid and zinc chloride activation, *Chem. Eng. J.*, 2010, **158**(2), 129–142.
53 A. Mancera, V. Fierro, A. Pizzi, S. Dumarçay, P. Gérardin, J. Velásquez, G. Quintana and A. Celzard, Physicochemical characterisation of sugar cane bagasse lignin oxidized by hydrogen peroxide, *Polym. Degrad. Stab.*, 2010, **95**(4), 470–476.
54 A. A. Tolba, Evaluation of uranium adsorption using magnetic-polyamine chitosan from sulfate leach liquor of sela ore material, South Eastern Desert, Egypt, *Egypt. J. Chem.*, 2020, **63**(12), 5219–5238.
55 L. Ali, A. Palamanit, K. Techato, A. Ullah, M. S. Chowdhury and K. Phoungthong, Characteristics of biochars derived

from the pyrolysis and co-pyrolysis of rubberwood sawdust and sewage sludge for further applications, *Sustainability*, 2022, **14**(7), 3829.

56 K. Kuśmierek, L. Dąbek and A. Świątkowski, The influence of the shape and grain size of commercial activated carbons on their sorption efficiency towards organic water pollutants, *Desalin. Water Treat.*, 2025, **321**, 100996.

57 B. Caballero-Mejía, A. Moliner, C. Escolástico, C. Hontoria, I. Mariscal-Sancho and J. Pérez-Esteban, Use of magnetite nanoparticles and magnetic separation for the removal of metal (loid) s from contaminated mine soils, *J. Hazard. Mater.*, 2025, **486**, 137081.

58 R. Jain, Recent advances of magnetite nanomaterials to remove arsenic from water, *RSC Adv.*, 2022, **12**(50), 32197–32209.

59 Z. Niu, S. Zhang, M. Ma, Z. Wang, H. Zhao and Y. Wang, Synthesis of novel waste batteries-sawdust-based adsorbent via a two-stage activation method for Pb2+ removal, *Environ. Sci. Pollut. Res.*, 2019, **26**(5), 4730–4745.

60 D. Mohan and K. P. Singh, Single-and multi-component adsorption of cadmium and zinc using activated carbon derived from bagasse—an agricultural waste, *Water Res.*, 2002, **36**(9), 2304–2318.

61 E. M. Soliman, S. A. Ahmed and A. A. Fadl, Reactivity of sugar cane bagasse as a natural solid phase extractor for selective removal of Fe (III) and heavy-metal ions from natural water samples, *Arabian J. Chem.*, 2011, **4**(1), 63–70.

62 A. Shukla, Y. H. Zhang, P. Dubey, J. L. Margrave and S. S. Shukla, The role of sawdust in the removal of unwanted materials from water, *J. Hazard. Mater.*, 2002, **95**(1–2), 137–152.

63 L. J. Yu, S. S. Shukla, K. L. Dorris, A. Shukla and J. L. Margrave, Adsorption of chromium from aqueous solutions by maple sawdust, *J. Hazard. Mater.*, 2003, **100**(1–3), 53–63.

64 A. Kheradmand, M. Negarestani, S. Kazemi, H. Shayesteh, S. Javanshir and H. Ghiasinejad, Adsorption behavior of rhamnolipid modified magnetic Co/Al layered double hydroxide for the removal of cationic and anionic dyes, *Sci. Rep.*, 2022, **12**(1), 14623.

65 M. Hema and K. Srinivasan, Uptake of toxic metals from wastewater by activated carbon from agro industrial by-product, *Indian J. Eng. Mater. Sci.*, 2010, **17**(5), 373–381.

66 R. G. Lehmann and R. D. Harter, Assessment of copper-soil bond strength by desorption kinetics, *Soil Sci. Soc. Am. J.*, 1984, **48**(4), 769–772.

67 D. A. Gkika, A. K. Tolkou, I. A. Katsoyiannis and G. Z. Kyzas, The adsorption-desorption-regeneration pathway to a circular economy: the role of waste-derived adsorbents on chromium removal, *Sep. Purif. Technol.*, 2025, **368**, 132996.

68 R. Gottipati, Preparation and characterization of microporous activated carbon from biomass and its application in the removal of chromium (VI) from aqueous phase, Doctoral dissertation, Department of Chemical Engineering, National Institute of Technology Rourkela, Odisha, India, 2012.

69 O. Hamdaoui, Batch study of liquid-phase adsorption of methylene blue using cedar sawdust and crushed brick, *J. Hazard. Mater.*, 2006, **135**(1–3), 264–273.

70 M. Alkan, Ö. Demirbaş and M. Doğan, Adsorption kinetics and thermodynamics of an anionic dye onto sepiolite, *Microporous Mesoporous Mater.*, 2007, **101**(3), 388–396.

71 Q. Li, Q. Y. Yue, Y. Su, B. Y. Gao and L. Fu, Cationic polyelectrolyte/bentonite prepared by ultrasonic technique and its use as adsorbent for Reactive Blue K-GL dye, *J. Hazard. Mater.*, 2007, **147**(1–2), 370–380.

72 M. Monier, M. A. Akl and W. M. Ali, Modification and characterization of cellulose cotton fibers for fast extraction of some precious metal ions, *Int. J. Biol. Macromol.*, 2014, **66**, 125–134.

73 S. Lian, Kinetic and thermodynamic studies on biosorption of Cu (II) by chemically modified orange peel, *Trans. Nonferrous Met. Soc. China*, 2009, **19**(5), 1365–1370.

74 D. Rameshraja, V. C. Srivastava, J. P. Kushwaha and I. D. Mall, Quinoline adsorption onto granular activated carbon and bagasse fly ash, *Chem. Eng. J.*, 2012, **181**, 343–351.

75 Y. Önal, C. Akmil-Başar, D. Eren, Ç. Sarıcı-Özdemir and T. Depci, Adsorption kinetics of malachite green onto activated carbon prepared from Tunçbilek lignite, *J. Hazard. Mater.*, 2006, **128**(2–3), 150–157.

76 Y. Kan, Q. Yue, S. Liu and B. Gao, Effects of Cu and CuO on the preparation of activated carbon from waste circuit boards by H3PO4 activation, *Chem. Eng. J.*, 2018, **331**, 93–101.

77 J. Yang, Y. Zhao, S. Ma, B. Zhu, J. Zhang and C. Zheng, Mercury removal by magnetic biochar derived from simultaneous activation and magnetization of sawdust, *Environ. Sci. Technol.*, 2016, **50**(21), 12040–12047.

78 S. K. Manikandan, P. Pallavi, K. Shetty, D. Bhattacharjee, D. A. Giannakoudakis, I. A. Katsoyiannis and V. Nair, Effective usage of biochar and microorganisms for the removal of heavy metal ions and pesticides, *Molecules*, 2023, **28**(2), 719.

79 C. Wu, Y. Yang, Y. Zhong, Y. Guan, Q. Chen, W. Du and G. Liu, Biological calcium carbonate enhanced the ability of biochar to passivate antimony and lead in soil, *Environ. Sci.: Processes Impacts*, 2023, **25**(8), 1365–1373.

80 J. Wu, T. Wang, Y. Zhang and W. P. Pan, The distribution of Pb (II)/Cd (II) adsorption mechanisms on biochars from aqueous solution: Considering the increased oxygen functional groups by HCl treatment, *Bioresour. Technol.*, 2019, **291**, 121859.

81 A. J. Santana, W. N. dos Santos, L. O. Silva and C. F. das Virgens, Removal of mercury (II) ions in aqueous solution using the peel biomass of Pachira aquatica Aubl: kinetics and adsorption equilibrium studies, *Environ. Monit. Assess.*, 2016, **188**(5), 293.

82 Z. Wang, D. Wu, G. Wu, N. Yang and A. Wu, Modifying Fe3O4 microspheres with rhodamine hydrazide for selective detection and removal of Hg2+ ion in water, *J. Hazard. Mater.*, 2013, **244**, 621–627.

83 M. Attari, S. S. Bukhari, H. Kazemian and S. Rohani, A low-cost adsorbent from coal fly ash for mercury removal from industrial wastewater, *J. Environ. Chem. Eng.*, 2017, **5**(1), 391–399.

84 A. Somayajula, A. A. Aziz, P. Saravanan and M. Matheswaran, Adsorption of mercury (II) ion from aqueous solution using low-cost activated carbon prepared from mango kernel, *Asia-Pac. J. Chem. Eng.*, 2013, **8**(1), 1.

85 S. Kushwaha, S. Sodaye and P. Padmaja, Equilibrium, kinetics and thermodynamic studies for adsorption of Hg (II) on palm shell powder, *World Academy of Science, Engineering and Technology*, 2008, **43**, 600–606.

86 G. D. Vuković, A. D. Marinković, S. D. Škapin, M. Đ. Ristić, R. Aleksić, A. A. Perić-Grujić and P. S. Uskoković, Removal of lead from water by amino modified multi-walled carbon nanotubes, *Chem. Eng. J.*, 2011, **173**(3), 855–865.

87 Z. Wu, Z. Cheng and W. Ma, Adsorption of Pb (II) from glucose solution on thiol-functionalized cellulosic biomass, *Bioresour. Technol.*, 2012, **104**, 807–809.

88 O. Moradi, M. Aghaie, K. Zare, M. Monajjemi and H. Aghaie, The study of adsorption characteristics Cu2+ and Pb2+ ions onto PHEMA and P (MMA-HEMA) surfaces from aqueous single solution, *J. Hazard. Mater.*, 2009, **170**(2–3), 673–679.

89 K. Nuithitikul, R. Phromrak and W. Saengngoen, Utilization of chemically treated cashew-nut shell as potential adsorbent for removal of Pb (II) ions from aqueous solution, *Sci. Rep.*, 2020, **10**(1), 3343.

90 S. Pap, V. Bezanovic, J. Radonic, A. Babic, S. Saric, D. Adamovic and M. T. Sekulic, Synthesis of highly-efficient functionalized biochars from fruit industry waste biomass for the removal of chromium and lead, *J. Mol. Liq.*, 2018, **268**, 315–325.

91 S. Cheung, Y. Cao and Q. Jiang, Study on removal of heavy metal pollution from water by biochar and its composite materials, *Highl. Sci. Eng. Technol.*, 2023, **40**, 227–232.

92 X. Huang, D. Wei, X. Zhang, D. Fan, X. Sun, B. Du and Q. Wei, Synthesis of amino-functionalized magnetic aerobic granular sludge-biochar for Pb (II) removal: Adsorption performance and mechanism studies, *Sci. Total Environ.*, 2019, **685**, 681–689.

93 L. Tang, J. Yu, Y. Pang, G. Zeng, Y. Deng, J. Wang, X. Ren, S. Ye, B. Peng and H. Feng, Sustainable efficient adsorbent: alkali-acid modified magnetic biochar derived from sewage sludge for aqueous organic contaminant removal, *Chem. Eng. J.*, 2018, **336**, 160–169.

94 M. Imran, Z. U. Khan, M. M. Iqbal, J. Iqbal, N. S. Shah, S. Munawar, S. Ali, B. Murtaza, M. A. Naeem and M. Rizwan, Effect of biochar modified with magnetite nanoparticles and HNO3 for efficient removal of Cr (VI) from contaminated water: a batch and column scale study, *Environ. Pollut.*, 2020, **261**, 114231.

95 Z. Madzin, I. Zahidi, M. E. Raghunandan and A. Talei, Potential application of spent mushroom compost (SMC) biochar as low-cost filtration media in heavy metal removal from abandoned mining water: a review, *Int. J. Environ. Sci. Technol.*, 2023, **20**(6), 6989–7006.